Systems/Circuits

Context-Dependent Inhibitory Control of Stimulus-Specific Adaptation

Tohar S. Yarden, Adi Mizrahi, and Israel Nelken

Department of Neurobiology, the Alexander Silberman Institute of Life Sciences and the Edmond and Lily Safra Center for Brain Sciences, Hebrew University, Jerusalem 91904, Israel

Stimulus-specific adaptation (SSA) is the reduction in responses to frequent stimuli (standards) that does not generalize to rare stimuli (deviants). We investigated the contribution of inhibition in auditory cortex to SSA using two-photon targeted cell-attached recordings and optogenetic manipulations in male mice. We characterized the responses of parvalbumin (PV)-, somatostatin (SST)-, and vasoactive intestinal polypeptide (VIP)-expressing interneurons of layer 2/3, and of serotonin receptor 5HT3a-expressing interneurons of layer 1. All populations showed early-onset SSA. Unexpectedly, the PV, SST, and VIP populations exhibited a substantial late component of evoked activity, often stronger for standard than for deviant stimuli. Optogenetic suppression of PV neurons facilitated pyramidal neuron responses substantially more (approximately ×10) for deviants than for standards. VIP suppression decreased responses of putative PV neurons, specifically for standard but not for deviant stimuli. Thus, the inhibitory network does not generate cortical SSA, but powerfully controls its expression by differentially affecting the responses to deviants and to standards.

Key words: **auditory cortex; electrophysiology; interneurons; mouse; optogenetics**

Significance Statement

Stimulus-specific adaptation (SSA) reflects the growing complexity of auditory processing along the ascending auditory system. In the presence of SSA, neuronal responses depend not only on the stimulus itself but also on the history of stimulation. Strong SSA in the fast, ascending auditory pathway first occurs in cortex. Here we studied the role of the cortical inhibitory network in shaping SSA, showing that while cortical inhibition does not generate SSA, it powerfully controls its expression. We deduce that the cortical network contributes in crucial ways to the properties of SSA.

Introduction

Neurons often reduce their responses to frequently occurring stimuli [standards (Ss)], yet retain responsiveness to other, rarely occurring ones [deviants (Ds)], an effect termed stimulus-specific adaptation (SSA; Ulanovsky et al., 2003). SSA was found in the auditory (Ulanovsky et al., 2003), visual (Movshon and Lennie, 1979; Müller et al., 1999), and somatosensory (Katz et al., 2006; Musall et al., 2015) modalities. In the auditory modality, it was observed in macaques (Fishman and Steinschneider, 2012), cats (Ulanovsky et al., 2003), rats (Malmierca et al., 2009; von der Behrens et al., 2009; Taaseh et al., 2011), mice (Anderson et al., 2009), gerbils (Bäuerle et al., 2011), bats (Thomas et al., 2012), and barn owls (Netser et al., 2011). Although SSA already occurs in the inferior colliculus (Duque et al., 2012; Shen et al., 2015), substantial SSA first appears along the fast, narrowly tuned lemniscal pathway in the primary auditory cortex (A1; Antunes et al., 2010).

SSA has been shown quantitatively to correlate with objective measures of prediction error in the sensory stream (Rubin et al., 2016). SSA complements the dependence of neural responses on the physical properties of the stimulus (e.g., tone frequency) with a dependence on statistical features of the sound sequence in

Received May 10, 2021; revised Feb. 4, 2022; accepted Mar. 26, 2022.

Author contributions: A.M. and I.N. designed research; T.S.Y. performed research; T.S.Y. and I.N. analyzed data; T.S.Y. and I.N. wrote the paper.

T.S.Y. was supported by the Israeli President Scholarship for Excellence and Innovation in Brain Research and by the Gatsby Charitable Foundation. A.M. was supported by European Research Council (ERC) consolidator grant (616063) and a personal grant of the Israeli Science Foundation (224/17). I.N. was supported by personal grants of the Israel Science Foundation (390/2013 and 1126/2018), by a United States-Israel Binational Science Foundation–National Science Foundation grant (2016-688), and by an advanced ERC grant (340063). A.M. holds the Eric Roland Chair in Brain Sciences. I.N. holds the Milton and Brindell Gottlieb chair in Brain Sciences. We thank the following people for their technical support, advice, and discussions: Dr. Mickey London, Dr. Inbal Goshen, Dr. Lior Cohen, Dr. Yishai Elyada, Dr. Gen-ichi Tasaka, Dr. Ido Maor, Dr. Avi M. Libster, Dr. Itai Hershenhoren, Dr. Dina Moshitch, Dr. Maciej M. Jankowski, Dr. Johannes Niediek, Dr. Elena Kudryavitskaya, Dr. Amit Vinograd, Dr. Yasmin Yarden-Rabinowitz, Amos Shalev, Vitaly Lerner, Dr. Adi Kol, Alex Kazakov, Ana Polterovich, Mor Harpaz, Omer Amsalem, Omri Gilday, and Haran Shani-Narkiss. We also thank Dr. Ashlan Reid from Cold Spring Harbor Laboratory for providing us the Arch construct, and Dr. Maya Sherman from The Edmond and Lily Safra Center for Brain Sciences Vector Core Facility for designing and producing the viruses used in this study.

The authors declare no competing financial interests.

T.S. Yarden's present address: Department of Neurobiology, School of Medicine, Stanford University, Stanford, California 94305.

Correspondence should be addressed to Israel Nelken at israel@mail.huji.ac.il.

https://doi.org/10.1523/JNEUROSCI.0988-21.2022

which this stimulus is embedded. Thus, in rat A1, some neurons respond more strongly to rare stimuli that break the regularity of the sensory environment ("true deviants") than to equally rare stimuli within a random context (Hershenhoren et al., 2014), a situation termed true deviance sensitivity. Human mid-latency potentials (which may reflect neuronal SSA) show a similar preference for deviant stimuli (Grimm and Escera, 2012). These potentials may be upstream of mismatch negativity, the main deviance-sensitive component of the human auditory event-related potentials. Thus, SSA may link neural responses with higher functions that are crucial for perception.

Mechanisms proposed for SSA include synaptic depression of feedforward synapses (Mill et al., 2011; Taaseh et al., 2011) as well as recurrent synapses (May et al., 2015; Yarden and Nelken, 2017), or spike rate adaptation (Puccini et al., 2007; Abolafia et al., 2011). However, the ubiquity and robustness of cortical SSA remains hard to account for (Yarden and Nelken, 2017).

Sound processing in cortex is subject to robust inhibitory control that contributes to frequency tuning, intensity tuning, and temporal precision (Wang et al., 2000, 2002; Wehr and Zador, 2003; Kaur et al., 2004; Tan et al., 2004, 2007; Kurt et al., 2006; Wu et al., 2006, 2008). Cortical inhibitory neurons are often divided into the following three, largely nonoverlapping populations: parvalbumin (PV)-, somatostatin (SST)-, and the serotonin receptor 5HT3a (HTR)-containing neurons. HTR neurons include a major subclass that expresses vasoactive intestinal polypeptide (VIP; Lee et al., 2010; Zeisel et al., 2015) and targets mostly SST (but also PV) neurons (Pi et al., 2013; Askew and Metherate, 2016).

The properties of PV and SST inhibition in A1 were studied *in vitro* (Levy and Reyes, 2012) and *in vivo* (Chen et al., 2015; Natan et al., 2015, 2017; Phillips et al., 2017). PV and SST neurons show SSA (Chen et al., 2015; Natan et al., 2015). Intense optogenetic suppression of PV neurons resulted in similar increases of standard and deviant responses (Natan et al., 2015). However, since elevated firing may result in strong adaptation and limited responsiveness (Gothner et al., 2021), such powerful perturbations may not reflect the role of inhibitory networks (Atallah et al., 2012; Phillips and Hasenstaub, 2016).

Here we refine and extend the characterization of the inhibitory landscape during SSA begun by Chen et al. (2015) and Natan et al. (2015). We describe in detail the expression of SSA in all four major populations of inhibitory interneurons in the supragranular layers of cortex—L1 inhibitory interneurons, as well as PV, SST and VIP containing interneurons in L2/3. We hypothesized that when using subtle optogenetic perturbations, inhibitory interneurons affect the responses of pyramidal neurons in a condition-dependent manner.

Materials and Methods

Experimental procedures

Animals. All experimental procedures were approved by the Hebrew University Animal Care and Use Committee. Hebrew University is an Association for Assessment and Accreditation of Laboratory Animal Care International-approved institution. Mice of the PV-Cre, SST-Cre, and VIP-Cre strains, and the Cre-dependent tdTomato reporter strains Ai9 and Ai14, were obtained from The Jackson Laboratory (stock #008069, #013044, #010908, #007909, #007914). Htr3a-Cre mice were obtained from Mutant Mouse Resource and Research Center (stock #036680-UCD). In the two-photon targeted patch recordings for characterizing the inhibitory populations, we used the following: 10 PV-Cre, Ai9 double-heterozygous male mice, 11–15 weeks old (PV × Ai9); 15 SST × Ai9 males, 9–14 weeks old; 16 VIP × Ai9 males, 8–12 weeks old; and 5 Htr3a × Ai14 males, 11–12 weeks old. In the optogenetic suppression experiments, we used the following: 29 homozygous PV-Cre males, 8–14 weeks old; 9 homozygous VIP-Cre males, 10–12 weeks old; and 1 VIP × Ai9 male, 13 weeks old.

Surgical procedure for electrophysiological experiments. Animals were anesthetized with isoflurane. For induction of anesthesia, mice were placed in a custom-made induction box and 4% isoflurane in 1.5 L/min of O_2 were pumped into the box [M3000 Vaporizer, LEI Medical (now Supera)] until the animal was deeply anesthetized (breathing rate dropped to <90 breaths/min, and there was no righting reflex). Then, animals were placed in a surgery apparatus with bars fixing the head at the temples. During the surgery, anesthesia was maintained using 1.5–2% isoflurane in 0.2 L/min O_2, delivered through a custom-made face mask, and evacuated using a Fluovac machine (Harvard Apparatus). Subcutaneous injections of carprofen (4 mg/kg, using 0.5 mg/ml saline; Norbrook) and lidocaine (0.12 ml of lidocaine HCl 0.2% solution; Rafa Laboratories) were given for pain reduction, and of saline (NaCl 0.9%, 0.12 ml; B. Braun) for preventing dehydration. Additional injections of saline, 0.05 ml at a time, were given 2 h after the first through a butterfly syringe inserted subcutaneously, and then approximately every 2 h. During the surgery, the rectal temperature was maintained at 35 ± 1°C using a heating pad (DC Temperature Controller, FHC). Animals were covered with a paper towel blanket to prevent heat loss and excess heating of the pad. A piece of the scalp covering the dorsal surface of the skull was removed, and the skull was scraped clean using a surgical scalpel, washed with saline, and scratched with a crisscross pattern to improve the traction of glue. A custom-made metal bar was glued using dental cement (Coral-Fix) mixed with three to four drops of histoacryl (B. Braun). After the cement hardened, the head was fixed using the metal bar. The skin covering the temporal bone was cut, and the temporal muscle was disconnected from the bone at its dorsal side, using a scalpel, to expose the temporal bone. The bone was scraped clean and washed with saline. A wall of dental cement was formed around the temporal bone from all sides except the ventral, to keep the brain and lens wet in later stages. An approximately semicircular craniotomy was performed over the auditory cortex using a biopsy punch (3 mm diameter; Integra Miltex) and a micromotor drill (model MH-1 70, Foredom). The brain was kept wet using extracellular solution (NaCl 142 mM, KCl 5 mM, $CaCl_2$ 2 mM, $MgCl_2$ 1 mM, D-glucose 10 mM, and HEPES 10 mM. The following reagents were used: NaCl, Bio-Lab; KCl, Frutarom; $CaCl_2 \cdot 2H_2O$, Merck; $MgCl_2 \cdot 6H_2O$, J.T. Baker; D-(+)-glucose, Riedel-de Haën; HEPES, Sigma Life Sciences); and, if necessary, cleaned gently using solution-soaked gelatin tampons (A. Levy Dental; or SPONGOSTAN).

Virus injections. In some of our animals (PV-Cre and VIP-Cre or VIP × Ai9), viruses for expression of archaeorhodopsin (Arch) in the Cre-expressing population and of a red fluorescent marker in pyramidal neurons were delivered into auditory cortex by stereotaxic injection. We used the following viruses: AAV2/9-EF1α-DIO-ss-Arch-eGFP-ER2-WPRE (AAV9-DIO-Arch). The construct was made by Ashlan Reid (the Anthony Zador laboratory at Cold Spring Harbor Laboratories; additions to the backbone are similar to those of the eArch3.0) and either AAV2/9-CaMKII-tdTomato (AAV9-CaMKII-tdT; gives cytoplasmic labeling of pyramidal neurons) or AAV2/9-CaMKII-H2B-mRuby2 (limits expression to cell nuclei). Viruses were produced at The Edmond and Lily Safra Center for Brain Sciences Vector Core Facility, Hebrew University of Jerusalem. The virus solution was prepared by dilution of the two viruses in PBS (Dulbecco's Phosphate-Buffered Saline, Biological Industries), with the final titers of 2.42×10^{12} for the AAV9-DIO-Arch, 2.8×10^{12} for the AAV9-CaMKII-tdT, and 5×10^{12} for the AAV9-CaMKII-H2B-mRuby2. This titer was found to provide viable and effective expression of the opsin during a limited period of time after the injection, and a transfection rate of ~70%. Increasing the titer further resulted in cell death in the Arch-expressing population.

Surgery for virus injection started as above. Synthomycine (chloramphenicol 5% eye ointment, Rekah Pharmaceutical Products) or Fucithalmic (fusidic acid 1% eye drops) was spread over each eye for keeping it moist. An incision was made in the scalp along the midline, from between the ears to between the eyes, and the skin was retracted using surgical string. The skull was scraped clean and washed with saline. The animal was aligned to the axes of the stereotaxic device, and

the bregma-λ (B-Λ) distance was measured. A small craniotomy was made in the left side of the dorsal surface of the skull [anteroposterior (AP), −2.7 mm; ML, 2.2 mm]. To account for variability between mice, the AP coordinate was multiplied by the ratio between the measured B-Λ distance and the distance of 4.2 mm cited in *The Mouse Brain in Stereotaxic Coordinates* atlas (Paxinos and Franklin, 2003), up to a precision of 0.1 mm. In our mice, this typically resulted in AP distances of 2.5–2.6 mm.

Pipettes for virus injection were pulled from glass capillaries (3.5 inches long; Drummond Scientific) on a P-2000 puller (Sutter Instrument) to a shape having a narrow shank several millimeters long. Tweezers were used to break the pipette tip under the binocular, and the pipette was filled with mineral oil and mounted on a Nanoject II Auto-Nanoliter Injector (Drummond Scientific). The virus solution was loaded into the pipette, and the pipette was driven into the brain at an angle of 51° to the normal using a controller (Scientifica; see Fig. 8*A*, compare). The solution was injected at two sites, with depths of 3.300 and 2.800 mm along the track. In each site, 28 pulses of 9.2 nl each were given at a rate of one pulse every 2 s, as controlled by a Master-8 device (A.M.P.I.). In each site, the pipette was left in place for 5 min before moving to the next site or out of the brain. After the pipette was taken out, the craniotomy was covered with bone wax (catalog #901, Surgical Specialties), and the scalp was stitched with a silk string (5–0 USP; Assut Sutures). Expression time was between 12 and 26 d.

Auditory stimuli. Stimuli were generated as waveforms in MATLAB (MathWorks) and converted to analog voltages (digital-to-analog converter on a PCI-6731 card, using a BNC-2110 shielded connector block; both from NI). The analog signal was attenuated (catalog #PA5, TDT) and presented through an ED1 Electrostatic Speaker Driver and an ES1 Free Field Electrostatic Speaker (both from TDT). The speaker was placed ~10 cm from the right ear of the mouse and shielded using a wire mesh. The sampling rate of the audio signals was 192 kHz.

Sound level was calibrated using a model 4939 microphone and a type 4231 Sound Calibrator (Brüel & Kjær) by playing a range of pure tones from 3 to 64 kHz. An attenuation of 0 dB corresponded to ~100 dB SPL.

Neural responses were usually first characterized using broad-band noise presentations. Noise stimuli were synthesized at a spectrum level of about $-50\,\mathrm{dB}/\sqrt{\mathrm{Hz}}$ relative to pure tones at the same attenuation level and presented at 0–70 dB attenuations. Next, the frequency sensitivity of each neuron was characterized by presenting blocks of pure tones: each block consisted of 24 tones with a duration of 50 ms and 10 ms linear ramps at the beginning and end, spaced logarithmically from 3 to 64 kHz. Tones were presented at a random order with an interstimulus interval of 1000 ms. Typically, 10 blocks were presented in sequence, each with its own random order of stimuli. Pure-tone blocks were presented at a high, suprathreshold sound intensity level (usually 0–20 dB attenuation) to obtain tuning curves wide enough to select tones for the Oddball protocols.

Once the frequency tuning of a neuron was found, a central frequency (CF) was selected between two tone frequencies (f1 and f2) that both evoked clear responses. To the extent possible, the two frequencies were selected to evoke similar responses, although this was not always the case. The tones f1 and f2 were located at distances of 20% from the CF and 44% from each other (f2/CF = 1.2, CF/f1 = 1.2, and Δf = f2/f1 = 1.44, equal to a difference of 0.53 octave between f1 and f2). Tones in the Oddball protocols, and controls were 30 ms long, with a 5 ms onset and offset ramps, and were presented with an interstimulus interval of 300 ms (the same parameters as used by: Taaseh et al., 2011; Hershenhoren et al., 2014; Polterovich et al., 2018).

We tested the responses to these tones in five conditions (see Fig. 2): a block of an Oddball protocol consisted of 5 deviant tones and 95 standard tones presented in a random order; Oddball f1 has f1 as the oddball, or deviant, tone, and Oddball f2 has f2 as the deviant. In the Rare protocols, each block was composed of 5 trials of f1 (Rare f1) or f2 (Rare f2) and 95 silent trials (in which no tone was presented), presented in a random order. In the diverse broad (DB) protocol, each block had five trials of f1 and five trials of f2. The other 90 trials were divided equally among nine tones, distributed such that their distances from each other and from f1 and f2 were all equal to 1.44, and their frequencies did not fall below 100 Hz or above 64 kHz. This set of five protocols was repeated several times for each neuron, each time with a different randomization of the stimulus sequences and of the order of protocols.

We included in our analysis only those neurons for which we had at least five repetitions of the protocol set (in the regular targeted-patch recordings) or four repetitions in the optogenetic experiments (where each block was followed by an identical block where light stimulation was added; see below). Each repetition in the optogenetic experiments included one pair of no-light and light blocks for each protocol type). This provided a total of 475 standard and 25 deviant, diverse broad, and rare trials for each frequency in the targeted-patch recordings; and a total of 380 standard and 20 deviant, diverse broad, and rare trials in each of the two light conditions (with and without laser) in the optogenetic experiments.

Imaging and electrophysiology. We followed the protocol of previously published work (Cohen and Mizrahi, 2015; Maor et al., 2016, 2019). Pipettes were pulled from borosilicate glass capillaries (outer diameter, 1.5 mm; wall thickness, 0.25 mm; with filament; Hilgenberg) on a PC-10 puller (Narishige) to give resistances of 3.1–4.5 MΩ (filled with extracellular solution). The electrode was an Ag/AgCl wire (Ag wire, 0.35 mm diameter; Sigma-Aldrich Israel; immersed beforehand in NaClO 6% for oxidation). Pipettes were mounted in a custom-made pipette holder connected to a CV-7B Headstage and a MultiClamp 700B Microelectrode Amplifier (Molecular Devices).

During the recording, animals were anesthetized with sevoflurane (1.8–2.3% in O_2; Piramal Medical Care; vaporization and control, SomnoSuite Low-Flow Anesthesia Delivery System, Kent Scientific). The oxygen and sevoflurane mixture was bubbled through doubly deionized water to prevent dehydration or stimulation of the breathing tracts because of dryness (Martenson et al., 2005; Ewald et al., 2011). Sevoflurane was delivered through a face mask (model OC-SFM, World Precision Instruments) placed close to, but not tightly on, the animal snout. The depth of anesthesia was monitored through the rate and pattern of breathing, as detected by a strain gauge placed under the animal (catalog #KFH-3–120-C1-11L1M2R, DMD-265–220 Bridge Amplifier, Omega). During recordings, the rectal temperature was maintained at 37.1 ± 0.8°C using a heating pad (DC Temperature Controller, FHC). The animal was covered with a paper towel blanket to prevent heat loss and excessive heating of the pad.

We performed cell-attached recordings (loose patch) under the two-photon microscope (Margrie et al., 2003; Cohen and Mizrahi, 2015; Tasaka et al., 2018). Pipettes were filled with extracellular solution (as above), to which was added Alexa Fluor-488 (final concentration, 50 μM; catalog #A10436, Thermo Fisher Scientific) for visualization. Imaging of auditory cortex was performed using an Ultima two-photon microscope from Prairie Technologies (Bruker), equipped with a 16× water-immersion objective lens (numerical aperture, 0.8; working distance, 3.0 mm; model LWD, Nikon). Two-photon excitation of the electrode and of the cell somata was performed at 920 nm (Mai Tai DeepSee Femtosec Laser, Spectra-Physics). The recordings were restricted to subpial depths down to ~440 μm, as documented by the multiphoton imaging software.

The A1 was initially approximately located based on skull features, which were drawn and/or photographed before making the craniotomy in each animal (Nishikawa et al., 2018), and the exact locations of penetrations were selected such that at depths of 200–300 μm the pipette tip will be located within A1, caudally to the high-frequency boundary with AAF (Anterior Auditory Field; pipettes were inserted at an angle of 55–56° from the normal). A1 was identified by the following physiological criteria: strong and fast local field potential deflections in response to sounds, or the presence of short-latency (approximately ≤20 ms), phasic, low-jitter responses. In some of our mice, OGB was injected into the tissue at the typical recording depth. The location of the green fluorescent stain in brain slices was compared with the location of A1 as identified by the histologic features and the absence of a granular layer in the DAPI staining. Typically, this was between −2.7 and −3.5 mm relative to bregma, confirming that our recordings were made in A1.

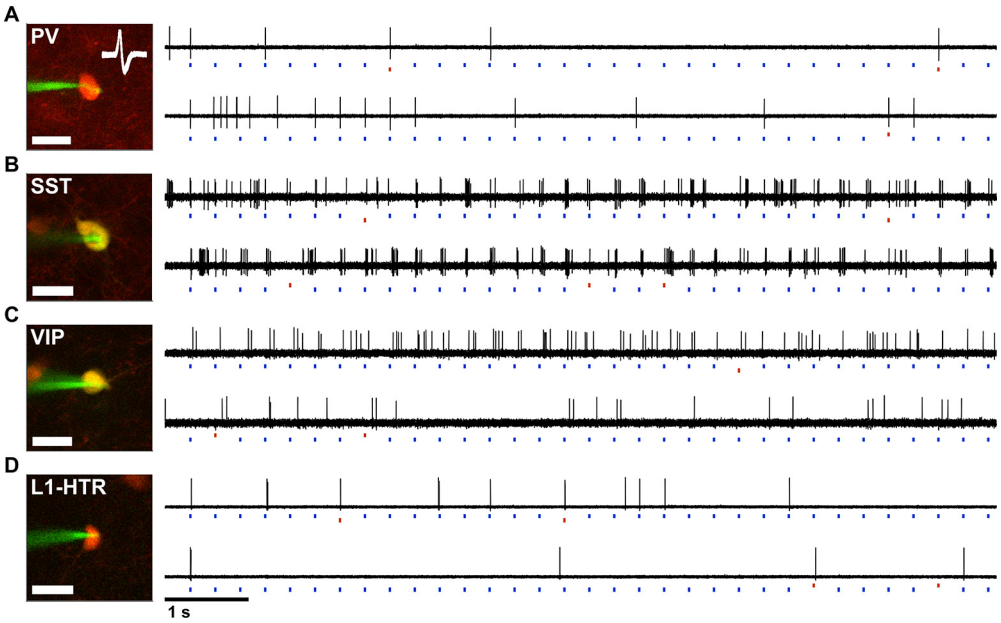

Figure 1. Targeted loose-patch recordings of inhibitory neurons in A1. ***A–D***, Left, Two-photon (2P) images of one recorded neuron from each population. Red channel shows the fluorescence of the transgenic tdTomato reporter; green channel shows the glass electrode filled with a fluorescent dye. In ***A***, overlaid white traces show the spike waveforms of the imaged neuron, confirming that it is a fast-spiking neuron. The somata of the SST and VIP neurons (***B***, ***C***) are yellow, indicating that they were filled with the pipette solution once the recording was finished, verifying the identity of the recorded neuron. Right, Voltage traces from the neurons in the 2P images, showing their spiking responses to the stimuli of the two Oddball protocols. In each protocol, two tones are presented: the standard tone (blue) with a high probability of occurrence (95%) and the deviant (red) with a low probability of occurrence (5%). The times and durations of the sound presentations are represented by colored patches below the traces. Vertical position corresponds to tone frequency: f1 (lower frequency) or f2 (higher frequency). Thus, the top row in each pair of traces shows an "Oddball f1" protocol, and the bottom an "Oddball f2" (compare Fig. 2). The average responses of the neurons shown here are presented in Figure 3. These neurons were selected for the early SSA they show (strong adaptation to the standards while preserving the responses to deviants) as well as for the availability of 2P images.

The glass pipette was driven into the cortex and navigated through the tissue using a PatchStar Micromanipulator (catalog #SCI-PS-700°C, Scientifica). Upon a successful penetration, the craniotomy was covered with two to three drops of agarose (2% in extracellular solution; High EEO, Sigma-Aldrich Israel) to suppress brain pulsations. The pipette was guided to neurons selected by their fluorescent labeling. Data acquisition was performed using the MultiClamp 700B Amplifier and a DigiData 1440A Digitizer (Molecular Devices).

The identification of inhibitory neurons of different populations relied on their labeling by the transgenic reporter. In PV-Cre mice, an additional criterion was the spike waveform (see below). In SST-Cre and VIP-Cre mice, further verification of the identities of targeted neurons was provided by filling them with dye: at the end of the recording from each neuron, a filling attempt was performed by increasing the pressure inside the pipette to 1–2 kPa and giving a "buzz" in the MultiClamp program, or by increasing the capacitance compensation to values that produced oscillations. In many cases, these measures broke the membrane and allowed filling of the neuron with the dye of the pipette solution, confirming that the recorded neuron was indeed the one initially targeted. Finally, the L1-HTR neurons were identified based on their cortical depths. Since all of our L1-HTR neurons were located within 115 μm of the pia mater (with only one of them deeper than 100 μm), they are most probably non-VIP, thalamic-input receiving neurons (Ji et al., 2016). Of our VIP neurons, only four were shallower than 150 μm (i.e., within L1), and those were similar in their properties to the rest of the VIP population.

Optogenetics. For optogenetic stimulation, light was delivered from an MGL-III-532–130 mW laser LED (CNI). The laser LED was connected to an optic fiber (diameter, 1500 μm; length, 1.5 m; Prizmatix), whose end was placed above the microscope and carefully positioned before each recording session such that the light entered the 16× lens centered and focused. Light intensity under the lens was typically measured up to ~30 mW/mm^2 (model PD300-BB-50mW sensor, NOVA II controller, Ophir Photonics). In blocks with light stimuli, light was presented around each stimulus, starting 20 ms before tone onset and ending 120 ms after tone offset (in one of our PV neurons, light offset was at 150 ms; see Fig. 8*D*). We always presented first a block with no light stimuli and then a block with the exact same stimulus sequence with light stimuli. In the Rare protocols, light was also applied on the silent trials to assess the effect of light on spontaneous activity and maintain conditions that are comparable to the other protocols.

Table 1. Population average responses

	Term	Df1	Df2	*F*	*p*
Early response range[a]					
ANOVA results	Condition	4	1543	302	7.8e-192
	Population	4	1543	0.912	0.46
	Condition/population	16	1543	33.5	3.1e-88
Late response range[b]					
ANOVA results	Condition	4	1543	15.7	1.3e-12
	Population	4	1543	7.26	8.6e-6
	Condition/population	16	1543	7.57	2.0e-17

Response, Mean firing rate within the specified time range; Condition, stimulus condition (standard, deviant, diverse broad, rare, or silence); Population, PV, SST, VIP, L1-HTR, or pyramidal; cell, identity of the neuron within the population; f, the identity of the tone frequency played (f1 or f2). All variables except Response are categorical. Responses were collected from 27 PV, 31 SST, 35 VIP, 24 L1-HTR, and 25 pyramidal neurons.
[a]Range: 0–30 ms for inhibitory populations, 0–40 ms for pyramidal neurons [model: Response ~ Condition * Population + (1|cell:f) + (Population|cell:f)].
[b]Range: 30–150 ms for inhibitory populations, 40–150 ms for pyramidal neurons [model: Response ~ Condition * Population + (1|cell:f) + (Population|cell:f)].

Data analysis

All the analyses were performed in MATLAB (MathWorks).

Data inclusion. We included in our datasets only those neurons that had a significant response to one of the three conditions (standard, deviant, or rare) for any of the two frequencies and during any of the response ranges (0–30, 30–150, and 0–150 ms following tone onset for the regular targeted recordings; and 0–40, 40–150, and 0–150 ms for the optogenetic suppression experiments, with the exception of fast-spiking (FS) neurons in the VIP-Cre mice, whose response ranges were 0–40, 40–100, and 0–100 ms; see under Statistics, below, for the choice of response ranges). Within each condition and frequency, significance was

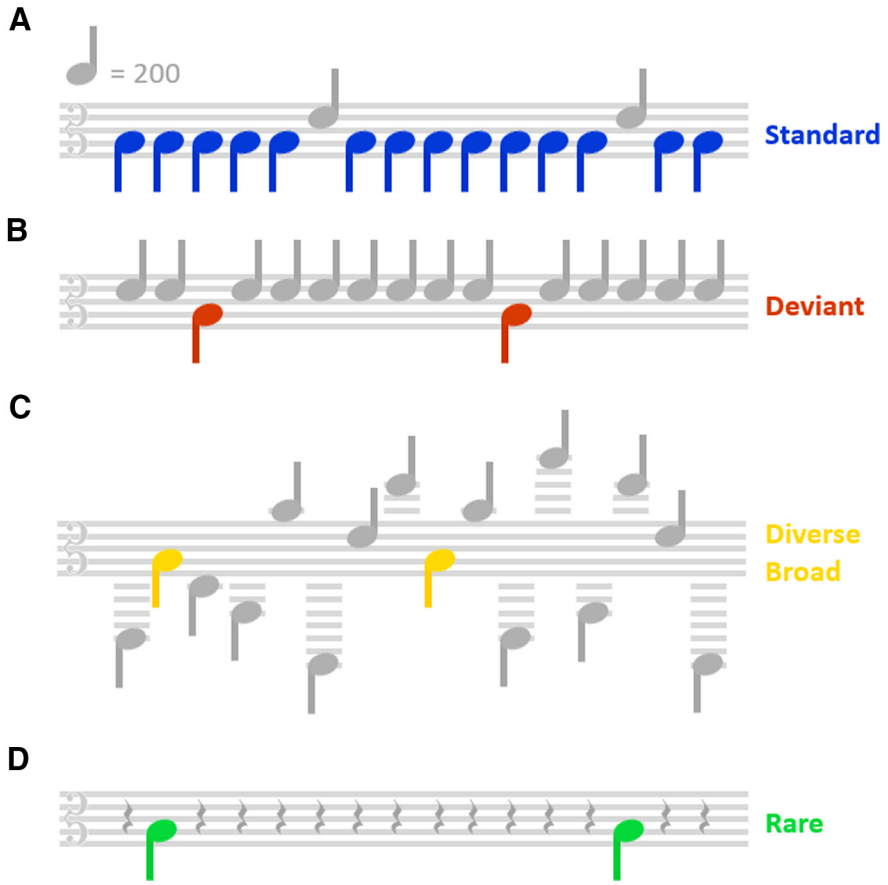

Figure 2. The Oddball protocols and controls. Tones are represented by musical notes. The vertical position of each note corresponds to tone frequency, and the implied musical intervals are approximately the same as those used in the experiments. ***A***, Specifics of the rate of presentation above the staff: 200 tones/min or one every 300 ms. The tones were 30 ms long, with 270 ms pauses between them, breaking somewhat the analogy with the musical notation. Each tone of the pair f1, f2 was presented in four different contexts, illustrated here for the lower frequency f1. ***A***, Standard (blue notes), occurring at high probability (95%) within a protocol that included the other tone of the pair (gray notes) as deviant. ***B***, Deviant (red), occurring at low probability (5%) within a protocol where the other tone was standard. ***C***, Diverse broad (yellow), where the two tones occurred with the same probability as the deviant in the Oddball protocols, but were interspersed randomly among ten other, equiprobable tones. All adjacent tones in this protocol had the same spacing as that between f1 and f2. ***D***, Rare (green), occurring at the same probability as the deviant but among trials with no tone presentations (represented by the crotchet rest). The full set of protocols included the following five sequences: Oddball f1 (***A***), Oddball f2 (***B***), Diverse Broad (***C***), Rare f1 (***D***), and Rare f2 (not shown).

tested by a paired *t* test (significance level, 0.05) on the firing rates (FRs) in all trials, comparing the rate within the response range to the rate during a baseline period (−50 to 0 ms for the regular targeted recordings, and −20 to 0 ms for the optogenetic suppression experiments). Thus, some neurons had a significant response to a tone and condition combination in one of the response ranges and not in others. In the optogenetic suppression experiments, the responses of a neuron at all conditions were included if the significance criterion was fulfilled in the no-light blocks or with any of the light intensities used during the recording from that neuron.

Spike-waveform classification. Neurons were classified as FS or non-FS using the following two parameters of the sorted waveforms: duration from peak to valley (t_{P2V}) and the negative valley-to-peak ratio (r_{-V2P}). We defined fast-spiking neurons as those with t_{P2V} <0.5 ms and r_{-V2P} >0.4 (similar in concept to the study by Cohen and Mizrahi, 2015). In the regular targeted recordings for characterizing the inhibitory populations, the waveform classification resulted in 1 PV neuron being classified as non-FS, and 1 VIP neuron and 1 L1-HTR neuron being classified as FS. These neurons were excluded from the analysis. In the optogenetic suppression experiments, we excluded FS neurons from the pyramidal neuron and VIP neuron datasets, and non-FS neurons from the PV dataset. Importantly, while the CaMKII promoter did label some FS neurons, it did not label any VIP neurons. Additionally, the non-FS CaMKII neurons showed typical waveforms that were different from those of our SST neurons, and never showed late responses.

Data analysis and statistics. Peristimulus time histograms (PSTHs) were calculated by binning the spike counts per trial into 1 ms bins, then smoothing the resulting histogram with a normalized Hamming window of length 10.

The time windows, or response ranges (also referred to as "response phases"), used in the analysis of neuronal responses (quantified by firing rate or spike counts) were determined according to the population average PSTHs. The PSTHs of inhibitory neuron populations showed an early response that lasted ~30 ms after tone onset, and a late response that started ~30 ms and ended by 150 ms after the tone onset (see Fig. 4). In the optogenetic suppression experiments, the time range for the early response was taken as 0–40 ms. This was meant to accommodate the longer early responses of pyramidal neurons, which at 30 ms were still not back at baseline (see Fig. 5*A*). Accordingly, the late range used was 40–150 ms, except for the fast-spiking neurons in the VIP suppression experiments, whose average late response terminated at ~100 ms and was followed by an additional wave of activity (ranges for these neurons, 0–40 and 40–100 ms). See Figure 5*B* for comparison of responses from both interneuron and pyramidal populations, using "Early" and "Late" as denominations for these response ranges.

The Common-Contrast SSA Index (CSI) was calculated according to the study by Taaseh et al. (2011): CSI = (Df1 + Df2 – Sf1 – Sf2)/(Df1 + Df2 + Sf1 + Sf2), where Df1 and Sf1 (Df2 and Sf2) are responses to f1 (f2) when D and S.

We used linear mixed-effects (LMEs) models to test the significance of the responses and then performed *post hoc* tests on specific contrasts, as described in the Results section and reported in the tables. The specific LMEs used are described in the corresponding tables. To improve the fit of the model to the data, we varied the random components of the models, as described below. When doing this, models were selected based on their Bayesian information criterion to provide the best fit to the data. Only the selected models were analyzed for the significance of fixed effects or contrasts.

Effects of light on neuronal activity (see Figs. 8-10, see Tables 7, 8, Using light as a categorical variable corresponding to the three light intensity bins sections) were analyzed by modeling the difference in firing rate responses (after baseline subtraction) between light and no-light conditions in different time ranges (usually 0–40, 40–150, or 0–150 ms after tone onset; see the main text for details). Light was used as a categorical variable, with values corresponding to the three light intensity bins (see Fig. 8).

The effect of PV suppression on the spontaneous activity of pyramidal neurons was analyzed using the difference between the firing rates (without baseline subtraction) in the light and no-light conditions for the silence condition, in the 0–150 ms range (this long range was taken because the rise in spontaneous activity appeared to develop slowly; see Fig. 9*I*, compare, see Table 8, Deviant and diverse broad responses only

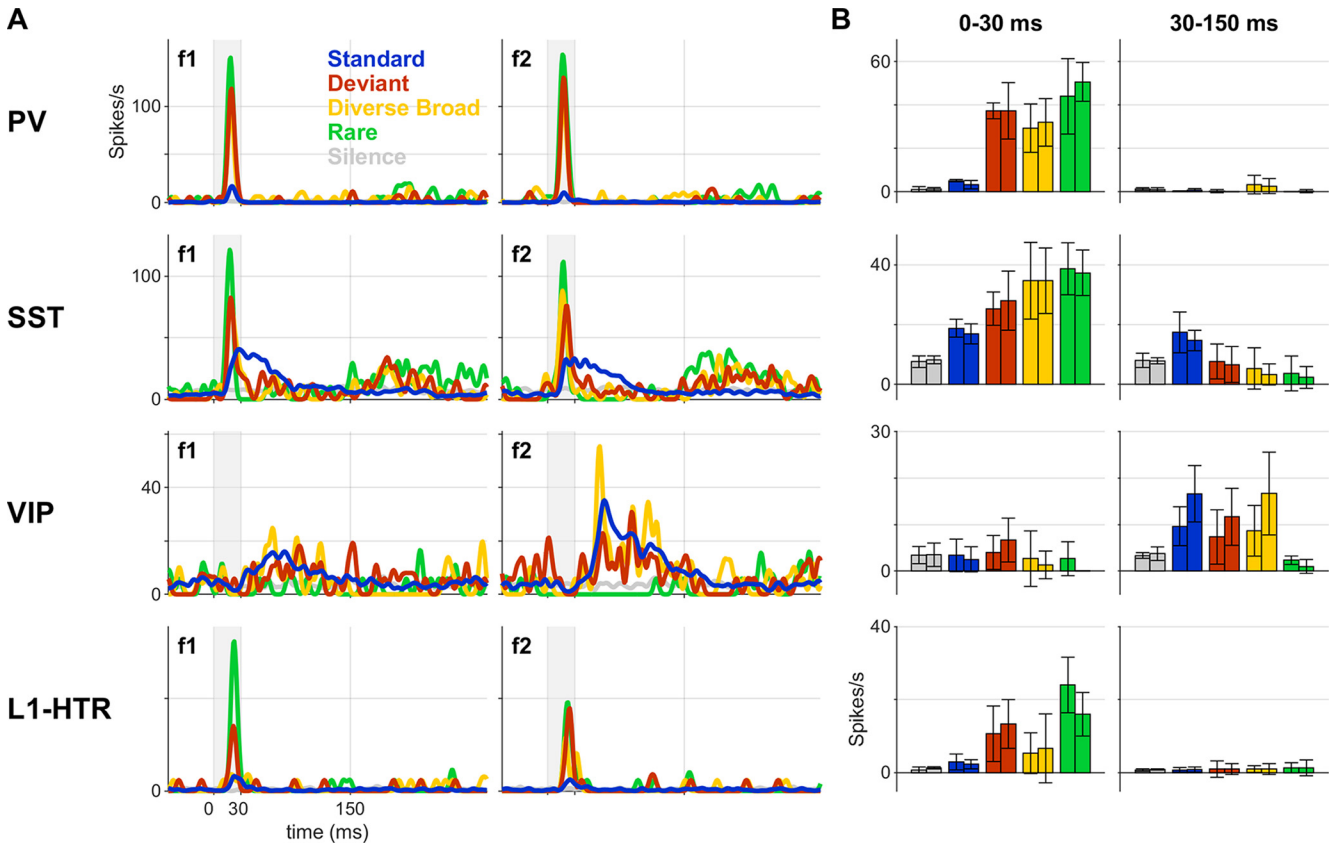

Figure 3. Responses of single PV, SST, VIP, and L1-HTR inhibitory interneurons. ***A***, Peristimulus time histograms for the responses of the neurons shown in Figure 1 to f1 (left column) and f2 (right), each presented in the four conditions depicted in Figure 2 for a total of 475 standard trials and 25 trials of each of the other conditions (deviant, diverse broad, and rare). A gray curve shows the activity during silent trials within the Rare protocol of the other frequency. Light gray patches mark stimulus presentations. The PSTHs were calculated with a resolution of 1 ms and smoothed with a 10 ms window. ***B***, Mean firing rates calculated for two phases of the response, 0–30 ms (left column) and 30–150 ms (right) after tone onset. Each pair of same-color bars shows the firing rates for f1 on the left and f2 on the right. Error bars show the SDs across the five blocks in which each protocol was presented. SDs (rather than SEs) are shown here to illustrate the variability of the responses across the five repetitions of each condition. The SEs would be 2.2 times smaller.

section). LMEs were also estimated for subsets of the data, for comparing the deviant and standard conditions as well as the deviant and diverse broad conditions [see Tables 7, Results for models run on subsets of the data (pairs of conditions) section, 8, Silence condition only, without baseline subtraction section].

To assess whether light had an effect on neuronal activity that was not because of the activation of Arch opsins (see Table 9), we used data recorded in animals that were not injected with the Arch virus (these were either noninjected animals or animals injected with the CaMKII-targeting virus only). Because of the smaller size of this dataset, all light intensities were lumped together.

VIP suppression was tested using the following model: difference ~ condition + (1|cell:f). Here, the large majority of the neurons was tested with the high-intensity range. In consequence, all light conditions were lumped together (see Tables 11, ANOVA statistics, 12, 13, ANOVA statistics for the data recorded from fast-spiking neurons and for pyramidal neuron data, including *post hoc* tests).

The time course of the standard responses during the block (see Fig. 11, see Tables 15, 16) was studied by modeling the average responses to specific pairs of trials as a function of the response range ("Range," 0–30 or 30–150 ms), pair identity ("Pair," the pairs composed of trials 1 and 2, 5 and 6, or 94 and 95), and the neuronal population ("Population"). The same model was fitted to the subset of the responses (cell–frequency pairs) that were significant in both the early and late responses ranges (see Fig. 11*B*, gray lines), and another model served for the whole response range (0–150 ms; see Table 14).

The time course of the effects of PV suppression on the pyramidal neurons (see Fig. 12, see Table 17) was studied by modeling the difference between the spike counts within the 0–40 ms range with and without light. Models were run separately for each population and for the standard and deviant conditions on data including the low and the high light intensity bins (low or high; see Fig. 8*H–J*, two extreme ranges).

Results

Two-photon targeted recordings in A1 from four inhibitory populations

To characterize the responses of inhibitory interneurons, we performed two-photon targeted loose-patch recordings in sevoflurane-anesthetized mice, from the four different populations of interneurons (Fig. 1): PV, SST, and VIP neurons of L2/3, and HTR neurons of L1 (L1-HTR). Inhibitory neurons were identified under the two-photon microscope by their expression of tdTomato (using PV-Cre, SST-Cre, VIP-Cre, and Htr3a-Cre crossed to Cre-dependent tdTomato reporter mice). Together, the PV, SST, and VIP populations, which are nonoverlapping, form ~75% of the total inhibitory interneuron population in L2/3 (Tremblay et al., 2016). Throughout this work, we will often refer to these populations collectively as "L2/3 interneurons." The L1-HTR neurons encompass >90% of the neurons in L1, which contains no PV neurons and only small fractions of SST and VIP neurons (Lee et al., 2010; Xu et al., 2010). Since HTR neurons are present in deeper layers as well, we limited their recordings to superficial depths.

We characterized the responses of these neurons to pure-tone stimuli at above-threshold sound levels. Based on the frequency tuning of the neuron, we selected two tones, f1 and f2, that evoked approximately similar responses and had a separation of

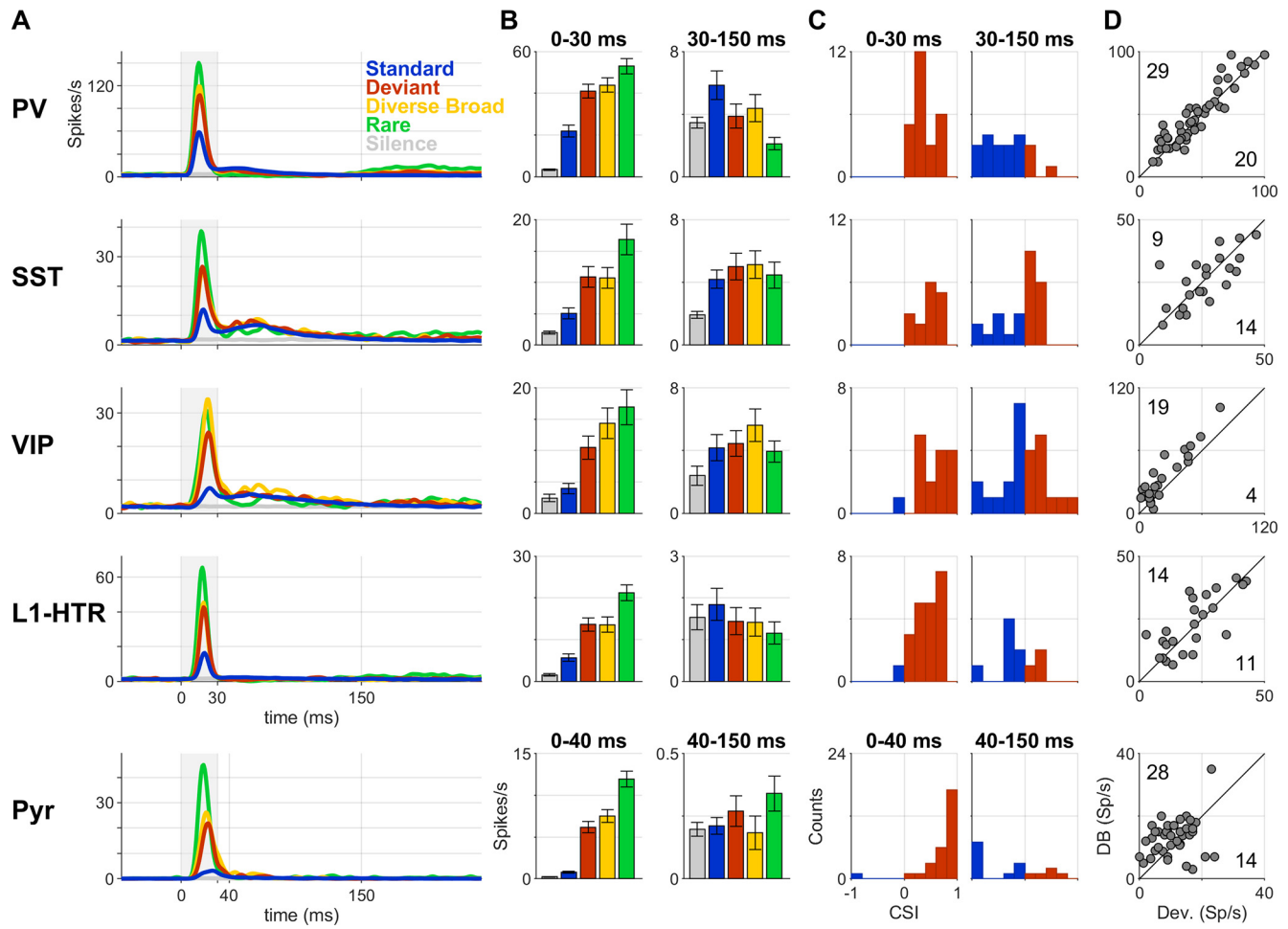

Figure 4. Early SSA and late anti-SSA in inhibitory and excitatory populations. ***A***, The average responses of all the neurons in each of the PV, SST, VIP, and L1-HTR populations, as well as the pyramidal population, presented as peristimulus time histograms. Responses are shown to tones in the four conditions (each condition averaged over the two frequencies f1 and f2). Gray curves show the average over silent trials. Light gray patches mark the stimulus. The PSTHs were computed at a resolution of 1 ms and smoothed with a 10 ms window. ***B***, Mean firing rates calculated for two phases of the response, 0–30 ms (left column) and 30–150 ms (right) after tone onset. Responses of pyramidal neurons are calculated for slightly different phases, 0–40 and 40–150 ms (set to accommodate the slower early phase of the evoked responses of these neurons; compare ***A***). Error bars show SEMs across the population. ***C***, Histograms of the CSI for each population in the two response phases. Bars are colored based on the preference for deviant (CSI $>$ 0, red) or standard (CSI $<$ 0, blue), showing only neurons with significant responses in the specified response phase. ***D***, Responses of each population to the DB condition versus the deviant condition (mean firing rate) in the early response phase (0–30 ms for inhibitory populations, 0–40 ms for the pyramidal). Each point represents the response of a neuron to one of the tones presented to it. Responses that are below the diagonal show a preference for "true deviants" over tones that are equally rare.

44% between them ($\Delta f = (f2 - f1)/f1$). These two tones were used to construct the Oddball protocols and controls (Fig. 2), consisting of five different protocols (Oddball f1, Oddball f2, Diverse Broad, Rare f1, and Rare f2), which together presented each of the two tones in a total of four different conditions, as follows: standard, deviant, diverse broad, and rare. Each protocol was presented as a block of 100 trials (one tone per trial, except for Rare protocols where most trials included no tone presentation). The probability of each tone to appear as a deviant in its corresponding Oddball protocol, as a rare tone in the Rare protocol, or within the Diverse Broad sequence, was 5% (five presentations in each block). Tone duration was 30 ms with 5 ms linear rise/fall ramps, and the interstimulus interval was 300 ms (onset to onset). We also measured the spontaneous activity of the neurons by using the silent trials of the Rare protocols, treating them as a fifth condition called "silence."

This sequence of blocks was repeated five times, with randomly permuted orders. To be included in the final dataset, neurons had to show a significant response to at least one of the two tones in the standard, deviant, or rare condition, in one of three response ranges (0–30, 30–150, and 0–150 ms following tone onset; see Materials and Methods); 28 PV ($N = 10$ mice), 31 SST ($N = 15$), 35 VIP ($N = 16$), and 24 L1-HTR ($N = 5$) neurons satisfied these criteria. The recorded neurons were all in the supragranular layers, and their depth underneath the cortical surface ranged between 213 and 398, 175 and 371, 86 and 438, and 20 and 115 μm, respectively.

Cortical interneurons show SSA

Inhibitory neurons showed a gradual reduction in the probability of evoked spiking to standard tones along the oddball sequence (Fig. 1*A*,*D*; the time course of the responses is further studied later in the section The time course of adaptation and facilitation in the inhibitory populations). Most of the neurons showed a short, well timed onset response that terminated within 30 ms (the tone duration). In this early response phase, the average responses to a tone when standard responses were almost always smaller than the average responses to the same tone when deviant (Fig. 3*A*, PSTHs for the PV, SST, and L1-HTR neurons, *B*, left column, corresponding bars).

Table 2. *Post hoc* comparisons for population average responses

Population	Contrast	Df1	Df2	*F*	*p*
Early response range					
PV	Dev > Std	1	1543	139	8.4e-31
	Rare > Dev	1	1543	54.7	2.3e-13
	Std > Sil	1	1543	131	3.8e-29
SST	Dev > Std	1	1543	14.8	1.2e-4
	Rare > Dev	1	1543	14.4	1.6e-4
	Std > Sil	1	1543	4.42	0.036
VIP	Dev > Std	1	1543	21.2	4.6e-6
	Rare > Dev	1	1543	22.8	2.0e-6
	Std > Sil	1	1543	0.239	0.63
L1-HTR	Dev > Std	1	1543	21.3	4.3e-6
	Rare > Dev	1	1543	19.6	1.0e-5
	Std > Sil	1	1543	5.86	0.016
Pyr	Dev > Std	1	1543	17.8	2.6e-5
	Rare > Dev	1	1543	20.2	7.5e-6
	Std > Sil	1	1543	0.181	0.67
Test					
$(Dev - Std)_{Pyr} - (Dev - Std)_{PV}$		1	1543	43.9	4.8e-11
$(Dev - Std)_{Pyr} - (Dev - Std)_{<PV,SST,VIP,L1\text{-}HTR>}$		1	1543	8.69	0.0032
Late response range					
PV	Dev < Std	1	1543	16.6	4.8e-5
	Std > Sil	1	1543	24.4	8.6e-7
	Dev > Sil	1	1543	0.750	0.39
SST	Dev > Std	1	1543	3.17	0.075
	Std > Sil	1	1543	29.4	6.9e-8
	Dev > Sil	1	1543	51.3	1.2e-12
VIP	Dev > Std	1	1543	0.404	0.52
	Std > Sil	1	1543	19.2	1.2e-5
	Dev > Sil	1	1543	24.8	7.0e-7
L1-HTR	Dev < Std	1	1543	0.602	0.44
	Std > Sil	1	1543	0.351	0.55
	Dev < Sil	1	1543	0.034	0.85
Pyr	Dev > Std	1	1543	0.0231	0.88
	Std > Sil	1	1543	0.00129	0.97
	Dev > Sil	1	1543	0.035	0.85

Dev, Deviant condition; Std, standard; Sil, silence; Pyr, pyramidal neurons. These coefficient tests were made on the model shown in Table 1. Responses were collected from 27 PV, 31 SST, 35 VIP, 24 L1-HTR, and 25 pyramidal neurons.
Early response range: 0–30 ms for Inhibitory populations, 0–40 ms for pyramidal.
Late response range: 30–150 ms for Inhibitory populations, 40–150 ms for pyramidal.

The L2/3 interneurons tended to have, in addition to or instead of the early response component, prolonged or late response components (Fig. 3, SST and VIP example neurons). The late response components of L2/3 interneurons were often stronger for the standard condition compared with the deviant (Fig. 3). We analyze here in detail the major component of the late responses, which lasted up to 150 ms after stimulus onset. PV neurons and SST neurons sometimes showed an even later wave of activity to low-probability tones (rare, diverse broad, and deviant), starting ~120 ms after tone onset (Fig. 3, example SST neuron; Fig. 6*G*, example PV neuron; 4*A*, population PSTHs for the PV and SST neurons). These very late responses were not very common and are not further analyzed here.

The existence of SSA in the early response phase (0–30 ms) in all populations, together with substantial activity in the late response phase (30–150 ms) of L2/3 neurons, is evident in the population average PSTHs (Fig. 4*A*) and in the average firing rates during these two response phases (Fig. 4*B*). The firing rates in the early response phase showed a significant main effect of stimulus condition, and a significant interaction between condition and neuronal population (Table 1, statistical reports for the LMEs; see Materials and Methods for details of the statistical tests and how they are reported).

Early standard responses (Fig. 4*A*, blue traces and bars) were weaker on average than the corresponding deviant responses (Fig. 4*A*, red) in all four populations (deviant > standard; Table 2, tests for the comparisons in the next paragraphs; unless stated otherwise, comparisons that are discussed in the main text were statistically significant). Almost all neurons showed standard responses that were smaller than their responses to the same stimuli when deviant. This is demonstrated by the CSI (see Materials and Methods), a measure that is commonly used to quantify the strength of SSA at the single-neuron level (Taaseh et al., 2011; Duque et al., 2012; Hershenhoren et al., 2014; Nieto-Diego and Malmierca, 2016). For the early response phase, almost all neurons that had significant responses also showed a positive CSI value, corresponding to the standard response being smaller than the deviant response [Fig. 4*C*, red bars in the CSI histograms (blue bars show negative CSI)].

In turn, the deviant responses were smaller on average than the rare responses (Fig. 4*B*, green; Rare > Deviant) in the early response phase, suggesting that deviant responses were partially adapted by the frequent presentation of the standard tone. This effect of the standard tone on the deviant responses is referred to later as cross-frequency adaptation.

Late phase responses showed significant main effects of condition and neuronal population, as well as a significant interaction between the two (Table 1). While the L1-HTR population did not show significant late responses in any condition, L2/3 populations had significant late responses in many conditions. Importantly, L2/3 interneurons had significant late responses to standards (standard > silence) that could be on average as large as the late deviant responses (in the SST and VIP populations) or even significantly larger (in the PV population). Indeed, in contrast to the ubiquity of SSA in the early phase of the responses, the late phase responses of most of the PV neurons, almost half of the SST neurons, and half of the VIP neurons showed standard responses that were larger than their deviant responses ["Anti-SSA": PV, 17 of 21 (84%); SST, 10 of 25 (40%); VIP, 13 of 25 (52%)]. This is the first report of such standard-preferring response components in primary auditory cortex.

We also recorded the responses of pyramidal neurons, reproducing the known SSA in this class of neurons (Fig. 5). In comparison with the inhibitory populations, pyramidal neurons had on average a larger difference between deviant and standard responses in the early response phase (Table 2) and, in consequence, higher CSI values (their distribution is heavily skewed toward 1). Pyramidal neurons showed almost no late activity.

Since true deviance sensitivity has been reported in rat auditory cortex (Taaseh et al., 2011; Hershenhoren et al., 2014; Polterovich et al., 2018), we were interested specifically in the relationships of the responses to the deviant and DB conditions (Fig. 4*D*, Table 3). The large range of frequencies in the DB sequence is expected to cause less cross-frequency adaptation than during the presentation of oddball sequences (Taaseh et al., 2011; Hershenhoren et al., 2014), so that stronger responses are expected in the DB than in the deviant condition.

The PV and VIP neurons clearly fulfilled this prediction in the early time range, and the VIP neurons showed the preference for the DB condition also in the late time range (Table 3). However, the SST and L1-HTR neurons differed significantly from the PV and VIP neurons in that they had on average equivalent responses in the DB and deviant conditions, violating the predictions of cross-frequency adaptation. Following the arguments of Taaseh et al. (2011), the SST and L1-HTR populations show true deviance sensitivity. One possible account for

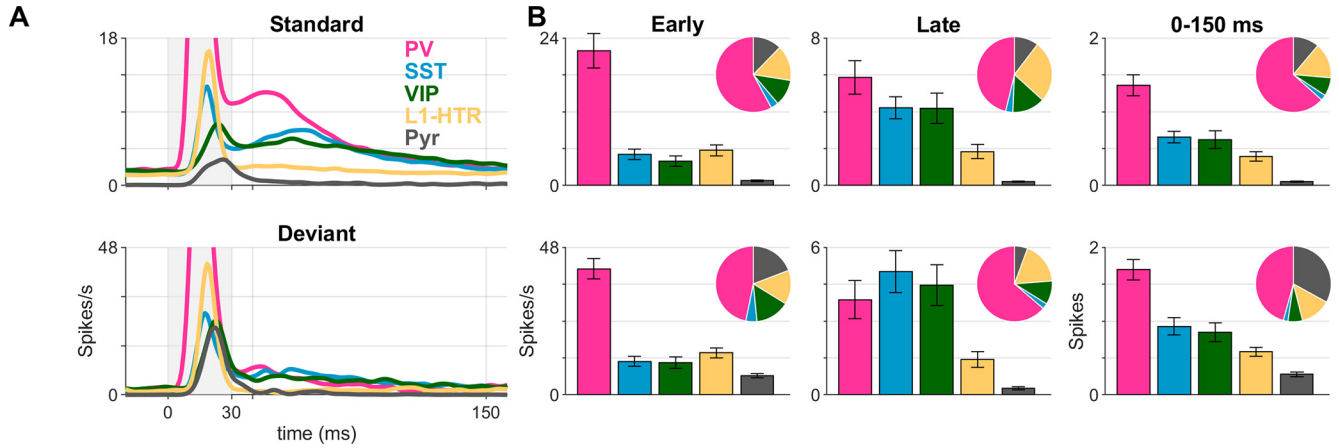

Figure 5. Comparison of evoked activity of the different inhibitory and excitatory populations. ***A***, PSTHs for the four populations of inhibitory neurons, plus the pyramidal neurons recorded in PV-Cre mice in the optogenetic manipulation experiments. Top, PSTHs for the standard condition. Bottom, PSTHs for the deviant condition. ***B***, Left and middle columns, Average firing rates (with SEs) for the five different neuronal populations, during the early response phase (0–30 ms for the inhibitory neurons, 0–40 ms for the pyramidal neurons; left) and the late response phase (30–150 ms for inhibitory neurons, 40–150 ms for pyramidal neurons; right), presented separately for the standard (top) and deviant (bottom) conditions. Right, Total spike counts (average ± SE) during the 0–150 ms range, for standard (top) and deviant (bottom). Inset, Pie charts show the calculated contribution of each population to the total spikes fired in L2/3 in response to each condition and in each response phase, based on the composition of L2/3 (Tremblay et al., 2016) and the probability of different cell types to respond to tones (Liang et al., 2019), and our own results, which were similar to their report for PV and pyramidal neurons. Our SST and VIP neurons had response probabilities similar to those of the pyramidal neurons, and L1-HTR neurons, similar to the PV neurons). In this calculation, we assumed 15% inhibitory neurons (INs) in the general population, and that the L2/3, non-VIP HTR neurons have the same probability to respond and the same response strengths as the L1 HTR neurons. Here, the orange bars and pie sections represent L2/3 non-VIP HTR neurons rather than L1-HTR neurons.

Table 3. Diverse broad and deviant responses

			Early range		Late range	
Term	Df1	Df2	*F*	*p*	*F*	*p*
ANOVA statistics						
Condition	1	630	11.7	6.6e-4	2.12	0.15
Population	4	630	41.1	1.3e-30	16.4	8.1e-13
Condition:population	4	630	5.02	5.4e-4	2.71	0.029
Coefficient tests						
DB ~ = Dev						
PV	1	630	11.7	6.6e-4	2.12	0.15
SST	1	630	0.0466	0.83	0.129	0.72
VIP	1	630	27.0	2.7e-7	13.9	2.2e-4
L1-HTR	1	630	8.52e-4	0.98	Hardly any late responses	
Pyramidal	1	630	3.87	0.050	in L1-HTR and Pyramidals	
$(DB - Dev)_{population\ 1} \sim = (DB - Dev)_{population\ 2}$ (PV and VIP) vs (SST and L1-HTR)	1	630	17.9	2.6e-5		

All conventions are as in previous tables. Responses were collected from 27 PV, 31 SST, 35 VIP, 24 L1-HTR, and 25 pyramidal neurons. Early range model: Response ~ Condition * Population + (1|cell:f). Late range model: Response ~ Condition * Population + (1|cell:f) + (Population|cell:f).

the true deviance sensitivity of the SST neurons is the inhibition they get from VIP neurons: since VIP neurons respond more vigorously to tones in the DB condition than in the deviant condition, they may bias the SST neurons in the opposite direction.

Figure 5 shows the activities of the different neuronal populations plotted together for the standard and for the deviant condition, illustrating the relative strength of the PV responses compared with all other populations, and the strength of the late activity in the inhibitory populations, in both conditions. These data allowed us to estimate the fraction of spikes contributed by each population to the total spiking activity in the cortex. To do so, we had to assume the probability of neurons to respond to tones in each population as well as the fraction of each population in L2/3 of auditory cortex. For response probability, we used our own estimates, verified against published estimates (Liang et al., 2019) that were rather similar to ours. For the fraction of each type within the cortex, we used estimates from the literature (Tremblay et al., 2016). The results are presented in Figure 5*B* as pie charts. Remarkably, we find that PV interneurons account for about half or more of the spikes for both standards and deviants, in both early and late responses phases. Pyramidal neurons account for less than one-third of the spikes evoked by deviant stimuli, when their responses are particularly strong, and less than one-fifth of the spikes evoked by standard stimuli, because of their strong adaptation by the standards.

Interneurons show variable combinations of early and late response components

Although the population PSTHs of the SST and VIP neurons were qualitatively similar to those of the PV neurons, individual SST and VIP neurons showed diverse response profiles. Some neurons had a pure early response (Fig. 6*A*,*D*), with virtually no activity in the late phase; other neurons showed both early and late response components (Fig. 6*B*,*E*), and some neurons only began their spiking responses around or following stimulus offset. The late responses of the two latter groups were not

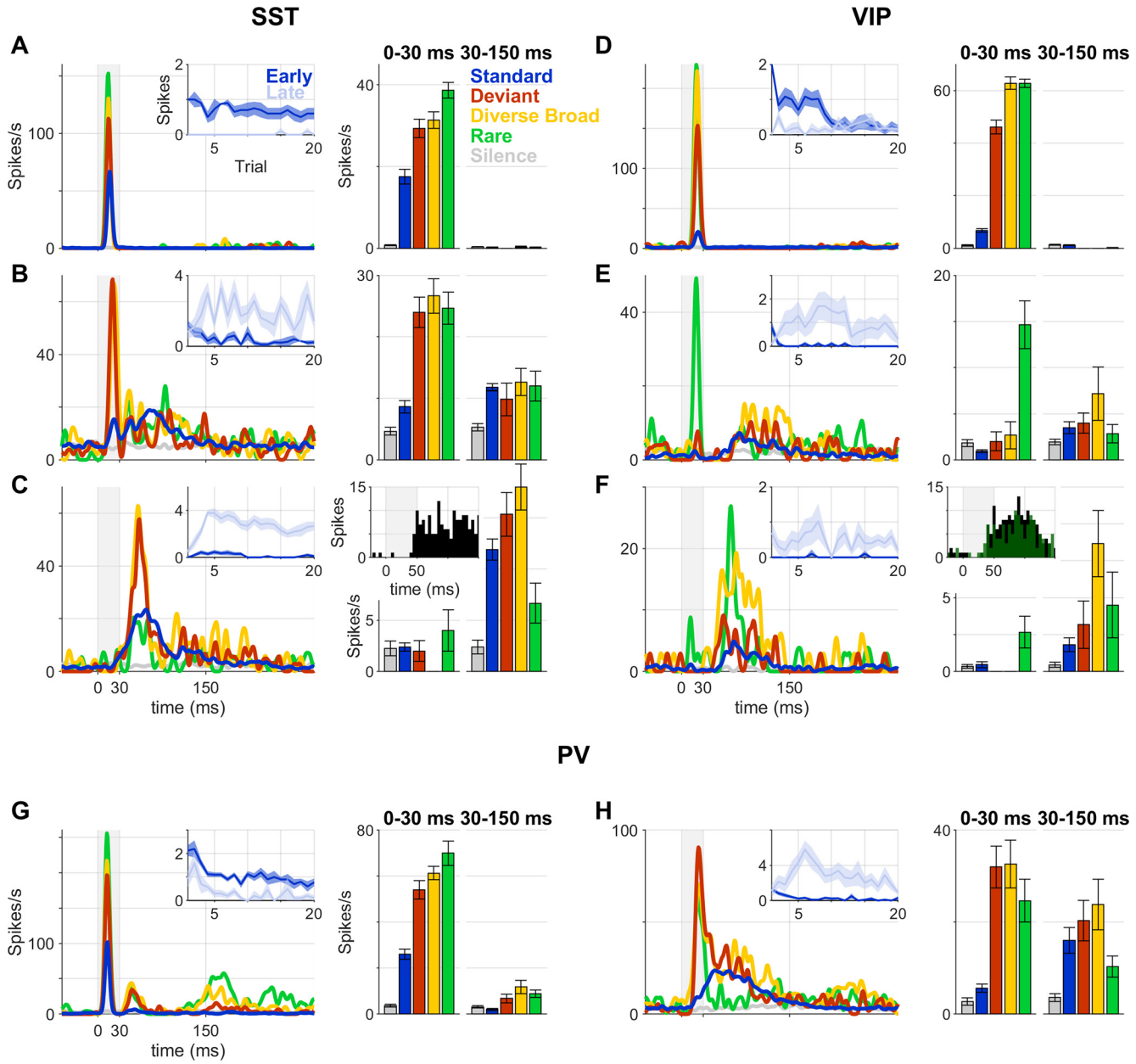

Figure 6. Heterogeneity of inhibitory neuron responses. ***A***, Left, Peristimulus time histogram for an example SST neuron with an early-onset response (same conventions as in Fig. 4). Inset, The time course of the early (0–30 ms, in blue) and late (30–150 ms, in light blue) components of the standard response of this neuron during trials 1–20. Bands show the SEM over a total of 10 blocks (5 for each frequency). Right panels, Mean firing rates during the early and late time ranges. Error bars show SDs across the five blocks in which each condition was presented. ***B***, Same as ***A***, for an example SST neuron with both early and late responses. ***C***, Same as ***A***, for an SST neuron with only a late response. The responses of this neuron to the 30 ms tones of the Oddball protocols were not offset responses: inset on the right shows the peristimulus time histogram of spikes evoked by 50-ms-long tone stimuli from 3 to 64 kHz (used for obtaining the tuning curve of the cell–see Materials and Methods. Spike counts are summed over responses to all tone frequencies). ***D–F***, Same as ***A–C*** for three example VIP neurons. The inset on the right-hand part of ***F*** shows the responses of this example neuron (black), as well as those of the example VIP neuron from Figures 1*C* and 3 (green). ***G***, ***H***. Same as above, for two-example PV neurons (early-onset response, ***G***; prolonged response, ***H***).

necessarily locked to sound offset: they were often also found at the same latencies in the pure-tone presentations used to obtain the frequency tuning of each neuron, where tone duration was longer (50 ms; Fig. 6*C*,*F*, insets). Thus, they are most likely long-latency responses to sound onset.

All PV neurons had early responses, and two-thirds also had a late response (19 of 27). Approximately 40–50% of the VIP and SST neurons lacked an early response and had only a late component (SST, 15 of 31; VIP, 14 of 35). Together with the neurons that also had an early response, approximately two-thirds of the SST and VIP neurons showed a late response (SST, 24 of 31; VIP, 23 of 35). In contrast with the L2/3 interneurons, L1-HTR neurons mostly showed pure onset responses (only 7 of 24 had late spikes, and only 1 had pure late spikes; these responses did not show significant differences relative to the spontaneous activity).

The time course of adaptation and facilitation in the inhibitory populations

To provide a concise profile of the time course of adaptation, Figure 7 shows the average responses to the first standard (S_1; usually the first trial of the block), to the standard that preceded the first deviant (SbD_1; this would be on average trial 19 of

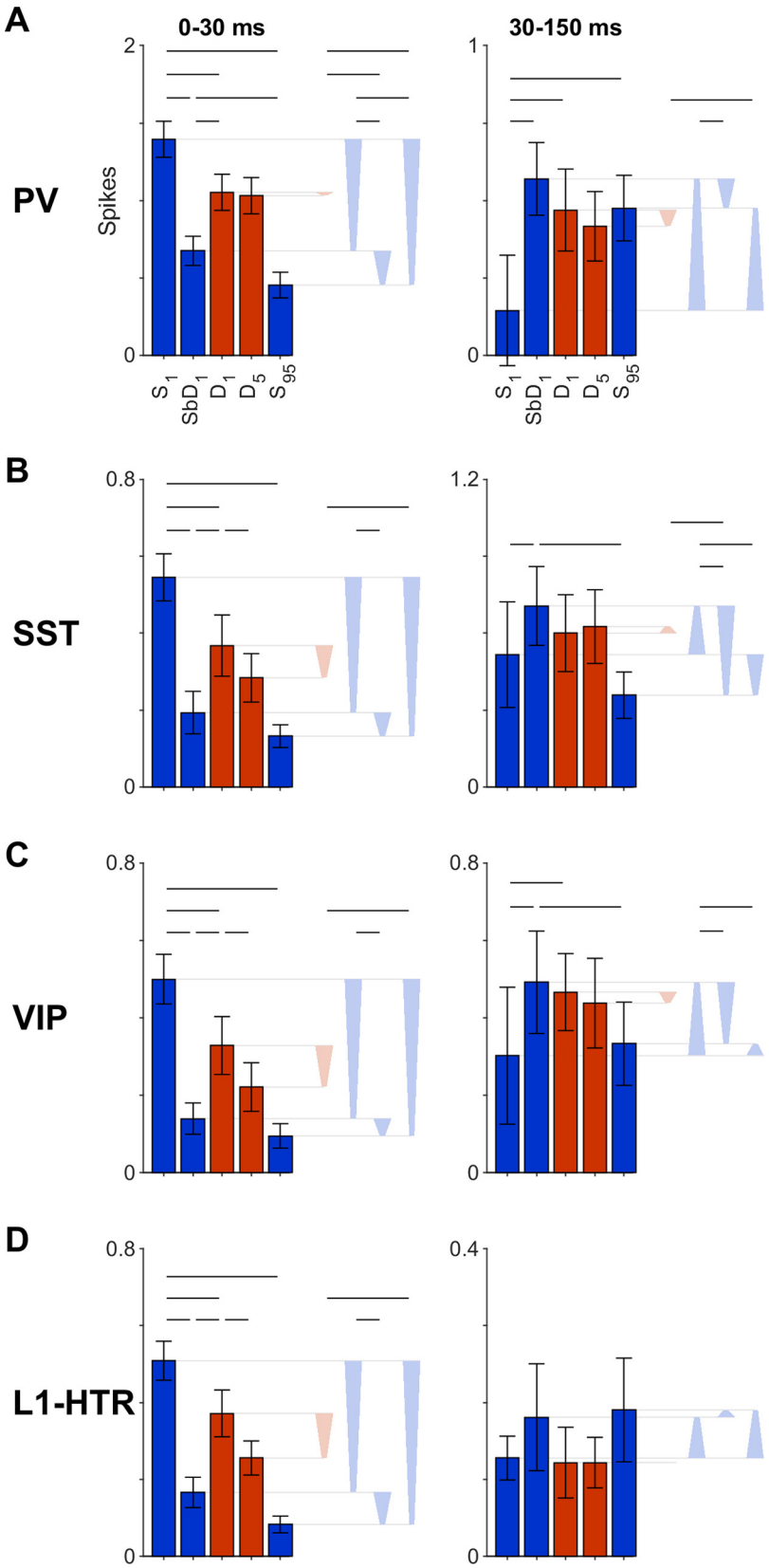

Figure 7. Time course of SSA in inhibitory populations. ***A***, The mean response of the PV population to the first standard tone (S_1), the standard tone just before the first deviant (SbD_1), the first and last deviants (D_1,D_5), and the last standard tone (S_{95}) within the block, in the early time range (0–30 ms, left column) and the late time range (30–150 ms, right). Error bars are SEMs. The set of trapezoids to the right-hand side of each plot shows the differences between pairs of trials from the main plot (the wide base of each shape marks the earlier stimulus within the block). In pink, first minus last deviant; in light blue, $S_1 - SbD_1$ (left), $SbD_1 - S_{95}$ (middle), and $S_1 - S_{95}$ (right). Horizontal bars above the plots mark significant differences (Tables 4-Tables 6, statistical details). ***B–D***, Same as ***A***, but for the other inhibitory populations.

the block, since the probability of the deviant was 5%), to the last standard (S_{95}), and to the first and last deviants in the block (D_1, D_5). The data were analyzed using a linear mixed-effects model (Table 4) and showed a significant main effect of trial type (reflecting the common time course of the SSA in all populations) and of population (reflecting the differences in response magnitude between them). There was also a significant interaction between trial type and population, reflecting small but significant differences in the adaptation profiles of the various inhibitory populations that will be highlighted below.

In the early response phase (Fig. 7, left column, Table 5), the standard responses decreased substantially between the first standard and the one preceding the first deviant ($S_1 > SbD_1$). The first deviant response tended to be smaller than the first standard response ($S_1 > D_1$), indicating the occurrence of cross-frequency adaptation, but was larger on average than the response to the standard just preceding it ($D_1 > SbD_1$). From that point on, both standard and deviant responses tended to decrease somewhat, by comparable amounts, up to the end of the block.

There were some variations between the populations in this general scheme. For example, while in all populations the average response decreased from SbD_1 to S_{95}, this additional decrease was significant only in the PV population ($SbD_1 > S_{95}$). On the other hand, the deviant responses decreased significantly from the first to last occurrence of the deviant within the block ($D_1 > D_5$) in all populations except for the PV neurons.

Remarkably, in the late phase (Fig. 7, right column, Table 6) the standard responses of the L2/3 populations were initially shaped by facilitation: all L2/3 populations showed significant response increases from the first standard tone to the standard preceding the first deviant ($S_1 < SbD_1$). This initial facilitation is further examined later in the article. Beyond that point, there were generally no significant differences in the responses to either standards or deviants—D1 was similar to SbD_1, and D_5 to D_1. Here too, there were small but significant population-specific variations. For example, in the SST and VIP populations, S_{95} was significantly smaller than SbD_1, so that in contrast with the PV population, the initial facilitation was largely wiped out by adaptation later in the block.

Table 4. Time course of SSA

ANOVA results	Term	Df1	Df2	*F*	*p*
Range 0–30 ms[a]	Population	3	6809	55.9	1.1e-35
	Type	4	6809	82.1	3.8e-68
	Population:Type	12	6809	8.46	3.9e-16
Range: 30–150 ms[b]	Population	3	6809	7.12	9.0e-5
	Type	4	6809	5.87	1.0e-4
	Population:Type	12	6809	2.36	0.0051

Response, The response in spikes; Type, the type of trial along the block (S_1, SbD_1, D_1, D_5, S_{95}); block, the identity of the block (protocols were played in 5 blocks of 100 trials). All other factors as defined previously. Responses were collected from 27 PV, 31 SST, 35 VIP, and 24 L1-HTR neurons, which provided 6829 observations that went into the models (responses of different neurons to different trial types and tone frequencies, in different blocks).
[a]Model: Response ~ Population * Type + (Population|cell:f) + (1|cell:block).
[b]Model: Response ~ Population * Type + (Population|cell:f) + (1|cell:block).

Table 5. *Post hoc* comparisons for time course of SSA in the 0–30 ms range

Coefficient tests results	Population	DF1	DF2	*F*	*p*
$S_1 > SbD_1$	PV	1	6809	216	3.0e-48
	SST	1	6809	52.3	5.4e-13
	VIP	1	6809	70.4	5.7e-17
	L1-HTR	1	6809	52.9	4.0e-13
$SbD_1 > S_{95}$	PV	1	6809	31.6	1.9e-8
$S_1 > D_1$	PV	1	6809	74.2	8.5e-18
	SST	1	6809	20.6	5.9e-6
	VIP	1	6809	24.1	9.2e-7
	L1-HTR	1	6809	12.2	4.7e-4
$D_1 > SbD_1$	PV	1	6809	91.8	1.3e-21
	SST	1	6809	19.7	9.1e-6
	VIP	1	6809	30.0	4.6e-8
	L1-HTR	1	6809	29.9	4.8e-8
$D_1 > D_5$	SST	1	6809	5.53	0.019
	VIP	1	6809	12.2	4.8e-4
	L1-HTR	1	6809	11.5	7.1e-4

Coefficient tests for the model in Table 4, early time range. The > and < signs are loosely used to indicate the sign of the comparison. Only significant effects are reported. Responses were collected from 27 PV, 31 SST, 35 VIP, and 24 L1-HTR neurons.

Table 6. *Post hoc* comparisons for time course of SSA in the 30–150 ms range

Coefficient tests results	Population	Df1	Df2	*F*	*p*
$S_1 < SbD_1$	PV	1	6809	18.8	1.5e-5
	SST	1	6809	4.53	0.033
	VIP	1	6809	4.97	0.026
$SbD_1 > S_{95}$	SST	1	6809	19.5	1.0e-5
	VIP	1	6809	5.11	0.024
$S_1 < D_1$	PV	1	6809	16.3	5.6e-5
	VIP	1	6809	5.81	0.016
$(D_1 - D_5) < (SbD_1 - S_{95})$	SST	1	6809	13.3	2.7e-4
$(D_1 - D_5) > (S_1 - S_{95})$	PV	1	6809	13.6	2.3e-4

Coefficient tests for Table 4, late time range. Same conventions as Table 5. Only significant effects are reported. Responses were collected from 27 PV, 31 SST, 35 VIP, and 24 L1-HTR neurons.

Optogenetic suppression of PV activity affected pyramidal responses in a condition-specific manner

To optogenetically suppress PV neurons, we injected a mixture of two viruses into A1 of PV-Cre mice: a Cre-dependent virus expressing the light sensitive opsin Arch, coupled to GFP as a fluorescent label, and a CaMKII-tdTomato or AAV9-CaMKII-H2B-mRuby virus to specifically label pyramidal neurons (see Materials and Methods). These injections resulted in a widespread labeling of PV and pyramidal neurons in L2/3 but not in L4, typically covering all of A1 (Fig. 8*A*,*B*). This pattern of expression, together with the strong attenuation of light intensity with depth, implies that that suppression of PV activity was effectively limited to neurons in L2/3. Thus, using targeted recordings from L2/3, we were able to probe both the opsin-expressing neurons and their postsynaptic targets (Fig. 8*C*). We recorded from a total of 13 Arch-expressing PV neurons and 25 pyramidal neurons (depth ranges, 95–381 and 141–306 μm).

Optogenetic stimulation of Arch (532 nM laser light, delivered through the lens of the two-photon microscope from 20 ms before to 150 ms after nominal stimulus onset, whether a stimulus was presented or, in silent trials of the rare condition, was not) caused a decrease in the spiking activity of PV neurons (Fig. 8*D*,*E*, Table 7, statistics). This decrease was observed across a wide range of light intensities: there was a significant difference between light and no-light conditions (Table 7, Using light as a categorical variable corresponding to the three light intensity bins section, significant effect of light; Table 7, Results for models run on subsets of the data (pairs of conditions) section, significant intercept). In almost all neurons tested with multiple laser intensities (five of six), responses decreased significantly with an increase in laser intensity.

Light reduced the PV activity mostly during the early phase of their responses (Table 7, Using light as a categorical variable corresponding to the three light intensity bins section); its effect on the late responses did not reach statistical significance. Paradoxical effects (i.e., enhancement of activity under light, were observed in 2 of 13 PV neurons; another 1 had a nonsignificant effect of light). Note that the ranges of early and late responses used here are 0–40 and 40–150 ms; 40 ms was found to demarcate early from late response components in pyramidal neurons and was used throughout for analyzing the optogenetic experiments. The effect of light on PV activity was similar for all conditions (except silence; Fig. 8*E*). Deviant and standard responses were affected similarly by light, as were deviant and diverse broad responses [Table 7, Results for models run on subsets of the data (pairs of conditions) section].

The responses of pyramidal neurons under light were significantly larger than without light (Fig. 9, Table 8, Using light as a categorical variable corresponding to the three light intensity bins section, "Light"). This effect was not because of a direct effect of the laser (tested by using laser in noninjected mice; Table 9). Furthermore, even at the highest laser intensity, pyramidal neurons did not develop late responses (Table 10).

PV suppression resulted in a differential increase of the responses of pyramidal neurons in different conditions (as demonstrated by the significant interaction between light and stimulus condition). Changes in firing rates are displayed in Figure 9*C*–*E* for the individual neurons, for standards and for deviants separately (Fig. 9*C*–*E*, blue and red, respectively), at three ranges of light intensity. While there is a clear increase in the firing rates for both standards and deviants (most points are above the diagonal), the size of the firing rate increases is much larger for the deviants (Fig. 9*C*–*E*, large differences in the ranges of the scatter plots). The average data for all tested conditions is plotted in Figure 9*F*–*H*, showing that firing rates increased more in the deviant than in the standard condition, while the responses in the deviant and diverse broad conditions increased to a comparable degree (Table 8, Silence condition only without baseline subtraction section, *post hoc* tests).

The difference between the effects of PV suppression on standard and deviant tones is illustrated in a different way in Figure 9, *I* and *J*, following the methods of Natan et al. (2015). Figure 9*I* (top) shows average time courses of the responses of pyramidal neurons tested at the highest light intensity range, each normalized to its own maximum FR in response to the

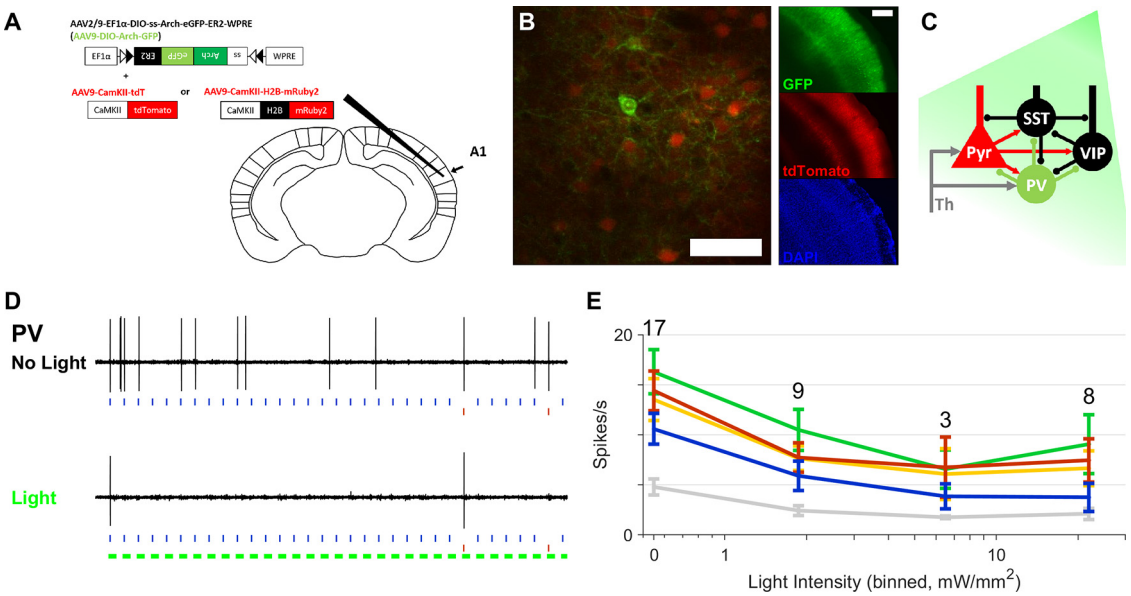

Figure 8. Selective expression of the arch opsin in PV neurons leads to the suppression of PV responses under light. ***A***, A mixture of viruses, AAV9-DIO-Arch-GFP and AAV9-CaMKII-tdTomato or AAV9-CaMKII-H2B-mRuby, was injected into A1 of PV-Cre mice. ***B***, Left, A two-photon image taken *in vivo* in A1 of a mouse expressing Arch-GFP in PV neurons and the red reporter tdTomato in pyramidal neurons. Scale bar, 50 μm. Right, Wide expression of the Arch and tdTomato in layer 2/3, covering all of A1 (fluorescence images from a brain slice: green and red channels on the top and middle panels, and blue on the bottom showing DAPI staining). Scale bar, 200 μm. ***C***, Schematic diagram of the cortical inhibitory circuit, with its main excitatory (arrows) and inhibitory (clubs) connections. PV and pyramidal neurons are colored according to the fluorophores used in our experiment. ***D***, Example traces from a PV neuron expressing Arch. Control responses to the Oddball protocol (top) are reduced in the presence of light (bottom). Blue and red patches mark the timing of standard and deviant tones, respectively. Green bars mark the timing of light pulses. ***E***, Light reduced firing in the PV population, in all of the conditions tested (mean and SEs of the firing rate 0–150 ms after tone onset).

Table 7. Effects of light on arch-expressing PV neurons, with binned light intensities

			Range 0–40 ms		Range 40–150 ms		Range 0–150 ms	
Term	Df1	Df2	*F*	*p*	*F*	*p*	*F*	*p*
Using light as a categorical variable corresponding to the three light intensity bins								
ANOVA results								
(Intercept)	1	193	6.04	0.015	3.32	0.070	4.16	0.043
Condition	4	193	3.06	0.018	4.39	0.0020	4.67	0.0013
Light	2	193	5.61	0.0043	1.60	0.20	3.18	0.044
Results for models run on subsets of the data (pairs of conditions)								
Deviant and standard responses only								
ANOVA results								
(Intercept)	1	78	4.90	0.030	6.05	0.016	4.20	0.044
Condition	1	78	0.0640	0.80	0.286	0.59	0.00832	0.93
Diverse broad and deviant responses only								
ANOVA results								
(Intercept)	1	78	6.20	0.015	5.71	0.019	6.00	0.017
Condition	1	78	2.02	0.16	0.657	0.42	1.97	0.16

Difference, Difference in mean firing rates between light and no-light conditions; Condition, stimulus condition (top: standard, deviant, diverse broad, rare, or silence; bottom: only two conditions at a time, as specified); Light, light intensity category (top); set, the identity of the protocol set (in some of the neurons, more than one set of oddball protocols and controls was played). Other factors are as defined in previous tables. Data are from 13 neurons. Model used: Difference ~ Condition + (1|cell:f) + (1|cell:set) + (1|cell).

deviant condition with no light. The bottom plots show the differences between the PSTHs in the light and no-light conditions. The average normalized firing rates are displayed in Figure 9*J*. The normalized firing rate changes are obviously much larger in the deviant than in the standard condition, illustrating again the substantially larger effects of PV suppression on the responses to deviants than on the responses to standards.

While the absolute changes in firing rate were substantially larger in the deviant than in the standard conditions, the proportional changes were more similar to each other, so that the effect of PV suppression could be multiplicative. Since the spiking responses of the pyramidal neurons to standard tones were almost fully adapted, it was hard to test this possibility with the available data, and it may be best tested using intracellular recordings.

PV responses were not totally abolished at the light intensities that we used. However, we refrained from using higher light intensities, because of the concern that adding spikes to the spontaneous activity of the pyramidal neurons would interfere with the course of adaptation. At the light intensities that we used, there was already a significant effect on the spontaneous activity of pyramidal neurons, although it was very small, as seen by the increased firing in the silence condition (Fig. 9, compare *I*, *J*, Table 8, Silence condition only, without baseline subtraction

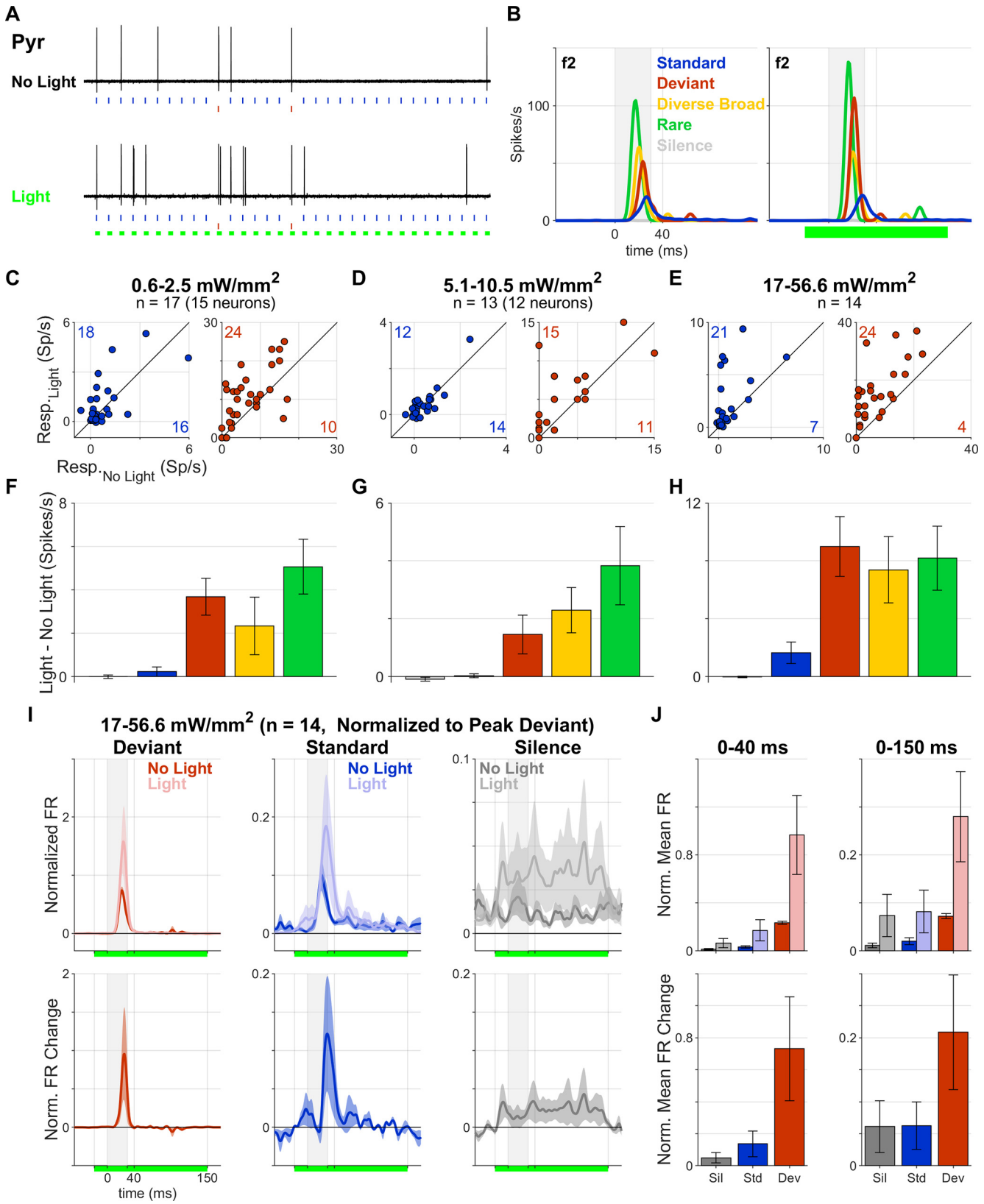

Figure 9. Optogenetic suppression of PV neurons increases responses of pyramidal neurons in a condition-dependent manner. ***A***, Example traces from a pyramidal neuron. Responses to the Oddball protocol (top) were enhanced in the presence of light (bottom). Blue and red patches mark the timing of standard and deviant tones, respectively. Green bars mark the timing of light pulses. ***B***, Peristimulus time histograms of the responses of the example neuron from F to tone f2 without (left) and with (right) PV suppression. Light gray patch marks the stimulus timing, and green bar shows the light pulse. ***C***, Scatter plots for the responses of pyramidal neurons to standard (left) and deviant (right) tones, with and without light, at the lowest range of light intensities used. Responses are mean firing rates in the range of 0–40 ms after tone onset. Data points represent the responses to each tone in each of the protocol sets played to different neurons (a few neurons were presented with two protocol sets with light intensities falling within the same bin—see numbers below the intensity range titles). Numbers on the plot areas show counts of responses enhanced by light (above diagonal) and responses reduced or unchanged (below diagonal). ***D***, ***E***, Same as ***C***, for the medium (***D***) and high (***E***) light intensity ranges. ***F***, Bars

Table 8. Effects of PV suppression on the pyramidal population

			Range 0–40 ms[a]	
Term	Df1	Df2	*F*	*p*
Using light as a categorical variable corresponding to the three light intensity bins[b]				
ANOVA results				
(Intercept)	1	433	31.3	3.9e-8
Condition	4	433	34.7	3.8e-35
Light	2	433	7.80	4.7e-4
Results for models run on subsets of the data				
Silence condition only, without baseline subtraction[c]				
ANOVA results				
Intercept	1	87	15.3	1.8e-4
Deviant and standard responses only[d]				
ANOVA results				
(Intercept)	1	174	46.9	12e-10
Condition	1	174	53.2	1.0e-11
Deviant and diverse broad responses only[e]				
ANOVA results				
(Intercept)	1	174	12.9	4.4e-4
Condition	1	174	2.16	0.14

Condition, Stimulus condition (top: standard, deviant, diverse broad, rare, or silence; bottom: only two conditions at a time, as specified). Other factors are as defined in previous tables. Data are from 25 neurons.
[a]At 40–150 ms, there were no significant responses, with or without light.
[b]Model: Difference ~ Condition + Light + (1|cell:f) + (1|cell:set) + (1|cell).
[c]Model: Difference ~ 1 + (1|cell:f) + (1|cell:set) + (1|cell).
[d]Model: Difference ~ Condition + (1|cell:f) + (1|cell:set) + (1|cell).
[e]Model: Difference ~ Condition + (1|cell:f) + (1|cell:set) + (1|cell).

Table 9. Effects of light in control mice

			Range 0–150 ms	
Term	Df1	Df2	*F*	*p*
ANOVA results[a]				
(Intercept)	1	65	0.476	0.49
Condition	4	65	0.574	0.68

Factors as described for previous tables. Data from five neurons (172–276 μm deep; two of them presented with two light intensities).
[a]Model: Difference ~ Condition + (1|cell:f).

Table 10. Late responses of the pyramidal population

			Range 40–150 ms	
Term	Df1	Df2	*F*	*p*
ANOVA results[a]				
(Intercept)	1	850	1.99	0.16
Condition	4	850	1.61	0.17
Light	3	850	0.149	0.93
Condition:light	12	850	0.623	0.82

All factors as described in previous tables. Data from 25 neurons.
[a]Model: Response ~ Condition * Light + (1|cell:f).

section). This small increase in pyramidal neuron spontaneous firing is in line with the decrease in spontaneous firing observed in the PV neurons under light (Fig. 8*E*, gray).

Suppression of VIP neurons caused a condition-specific reduction in the responses of postsynaptic targets

We expressed Arch in VIP neurons (Fig. 10*A*) and verified that light caused a reduction in their activity (Fig. 10*B*,*C*; seven Arch-expressing VIP neurons, 105–280 μm below surface). The difference between light and no-light conditions was significant for the 0-40 ms phase (Table 11, significant intercept), and all conditions were affected by the light to a similar degree (no main effect of condition). VIP late activity was not significantly affected by light at the light intensities used here.

VIP neurons mostly target other inhibitory interneurons, in particular SST neurons. Accordingly, we observed changes in the responses of fast-spiking neurons (11 presumed PV neurons; depth range, 198–317 μm) when suppressing the VIP neurons. There was a significant reduction in the firing of the fast-spiking neurons (Fig. 10*D*,*E*), with a significant main effect of stimulus condition in the 0–40 ms phase (Table 12). The suppression of VIP neurons reduced the responses of fast-spiking neurons in the standard and in the diverse broad conditions (Fig. 10*F*,*G*, Table 12, statistics), but did not significantly affect their deviant or rare responses. Importantly, the difference between standard and deviant responses, and between deviant and diverse broad responses, was significantly altered under light. These results suggest that these effects were largely because of disinhibition of the SST neurons, which are inhibited by the VIP neurons and in their turn inhibit the PV neurons.

←

showing the average difference between responses of pyramidal neurons with and without light for the different conditions, in the same light intensity range as ***H***. Error bars show SEMs over all responses. ***G***, ***H***, Same as ***F***, for the medium (***G***) and high (***H***) light intensity ranges. ***I***, ***J***, These panels follow the analysis performed in the study by Natan et al. (2015, their Fig. 4). ***I***, Top row, Peristimulus time histograms for the responses of pyramidal neurons in protocols using our highest light intensity range, normalized to the maximum firing rate (FR) of each neuron in response to the deviant condition under no light. Showing responses with (lighter colored curves and patches) and without light (darker colors) to the deviant (left), standard (middle), and silence (right) conditions. The latter is taken from the silent trials in the Rare sequences. Bottom row, The change in normalized FR because of the light (Light – No Light FRs), for the deviant, standard, and silence conditions (left, middle, and right panels, respectively). Light gray patch marks the tone duration, and green bars marks the light pulse. Bands around the traces show SEM. ***J***, Top row, The mean normalized FR along the 0–40 ms range (left) and the 0–150 ms range (right) after tone onset, showing responses to silence (Sil), standard (Std), and deviant (Dev) conditions under no light and under light, with the same color code as in ***I***. Bottom row, Mean change in normalized FR because of light (Light – No Light FRs) along the same time ranges as the top row. Error bars are SEMs.

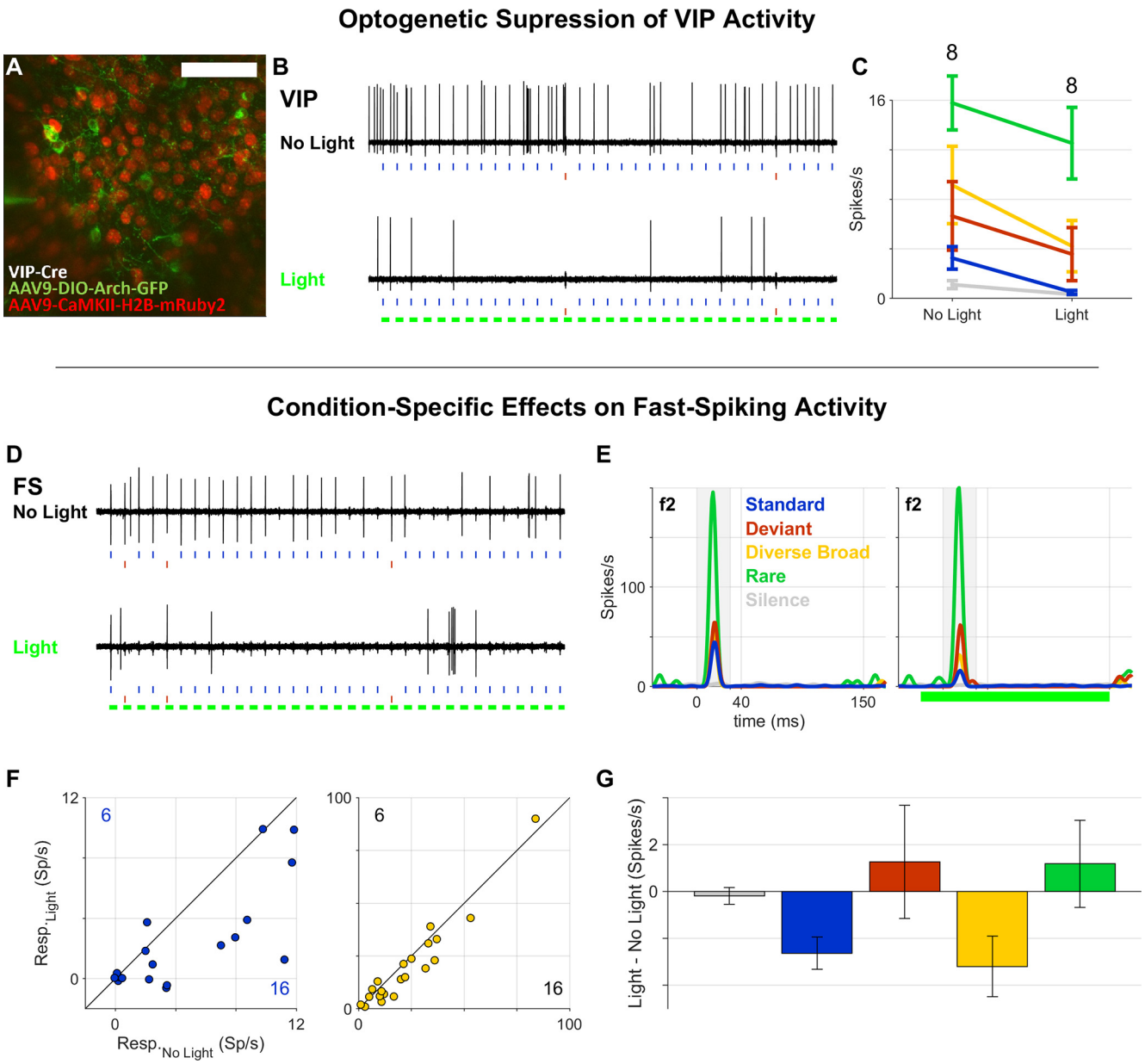

Figure 10. Condition-dependent effects of optogenetic suppression of VIP neurons. ***A***, A two-photon image taken *in vivo* in A1 of a mouse expressing Arch-GFP in VIP neurons and the red reporter mRuby2 in the cell nuclei of pyramidal neurons. Scale bar, 50 μm. ***B***, Example traces from a VIP neuron expressing Arch. Control responses to the Oddball protocol (top) are reduced in the presence of light (bottom). ***B***, ***D***, Blue and red patches mark the timing of standard (***B***) and deviant (***D***) tones, respectively. Green bars mark the timing of light pulses. ***C***, Light reduced firing in the VIP population, in all of the conditions tested (mean and SEs of the firing rate 0–40 ms after tone onset). ***D***, Example traces from an FS neuron. Control responses to the Oddball protocol (top) were reduced in the presence of light (bottom). ***E***, Peristimulus time histograms for the responses of the example neuron from ***D*** to tone f2 without (left) and with VIP suppression (right). Light gray patch marks the stimulus timing, and green bar shows the light pulse. ***F***, Scatter plots for the responses of fast-spiking neurons to the standard (left) and diverse broad (right) conditions, with and without light. Responses are the mean firing rates in the range of 0–40 ms after tone onset. Numbers on the plot areas show counts of responses enhanced by light (above diagonal) and responses reduced or unchanged (below diagonal). ***G***, Bars showing the average difference between responses of FS neurons with and without light for the different conditions. Error bars show SEMs over all responses. Standard and diverse broad responses were significantly reduced by the light, in contrast to the deviant and rare responses (Table 12).

We also recorded the responses of nine pyramidal neurons with and without optogenetic suppression of the VIP population (depth range, 211–323 μm). The pyramidal population showed a general decrease of standard, deviant, and diverse broad responses on VIP suppression, although this reduction was not statistically significant (Table 13).

Early dynamics of inhibitory interneurons

We found that some of the effects we describe here accumulated during the first few trials of the stimulation sequence. In particular, the facilitation of the late response components of layer 2/3 interneurons (Fig. 7), as well as the increase in the responses of pyramidal neurons following optogenetic suppression of PV interneurons (Fig. 9), both showed such a buildup.

The late response components of layer 2/3 interneurons often increased during the first few trials of the block (Fig. 7). The different dynamics of the early and late components are demonstrated by the dark and light blue curves in the insets of Figure 6.

To quantify the change in the responses during the first few standard presentations, we compared the average response of each neuron to trials 5 and 6 (in all cases where these trials were standard tone presentations; denoted <5,6>; trials that contained

deviants were excluded from the averaging) with the average response to trials 1 and 2 (when these were standard tone presentations; denoted <1,2>). These were calculated separately for each tested frequency, because both the response strength and the adaptation and facilitation dynamics could be different for the two frequencies (thus, each neuron may be represented twice in this analysis, if the f1 and f2 stimuli selected for it evoked a significant response, or once if only one of the tone frequencies evoked a significant response). The difference between <5,6> and <1,2>, denoted Δ_{III-I} (so named since it is the difference between the responses to the third and the first pairs of trials), was calculated for both the early (0–30 ms) and the late (30–150 ms) response phases.

Our main finding is that in the late time window, there was a significant increase in the spike counts between the first and third pairs of trials (Fig. 11*A*,*B*). This is in contrast to the early time window, where the spike counts showed a decrease, as expected from SSA (Fig. 11*B*). In consequence, there was no significant change in spike count over the 0–150 ms range between the first and third pairs of trials for any of the four neuronal populations (Table 14). Thus, at least at the population level, during the first few standard presentations there was a redistribution of spikes between the 0–30 ms and 30–150 ms time ranges, rather than a change in their total number. To show this redistribution of spikes, the data are analyzed here in terms of spike counts rather than as rates despite the differences in duration between the two response phases.

The early responses had on average a negative Δ_{III-I}, reflecting the adaptation of the early responses (Fig. 11*B*, Table 15) with approximately the same size in all interneuron populations (the interaction between pair and population was not significant). Single neurons largely conformed with this average behavior: 80% of the cases showed this decrease. In contrast, the late responses of the L2/3 populations had on average a positive Δ_{III-I} (Fig. 11*B*). The increase in the late responses to standards occurred in about two-thirds of the individual L2/3 neurons (Fig. 11*A*). Finally, Δ_{III-I} values were significantly different between the early and late phases in all L2/3 interneuron populations (Fig. 11*B*, Table 15). Limiting the analysis to neurons that had significant responses in both early and late phases, in most cases Δ_{III-I} was larger in the late phase than in the early phase, often turning from negative to positive (Fig. 11*B*, gray lines, Table 16).

As suggested in Figure 7, following the initial facilitation there was a decrease in the responses of the L2/3 populations. In all populations, the average responses to trials 94 and 95, when these contained standard presentations, were usually smaller than the responses to trials 5 and 6 (Table 14).

A similar buildup occurred in the responses of pyramidal neurons to optogenetic suppression of PV interneurons. Interestingly, during the first trials of the block the average response of pyramidal neurons was not affected much by light. The effect of light became pronounced only after the first 10 trials or so (Fig. 12*A*). This temporal dependence was observed in both the standard and deviant conditions: we collected the standard presentations occurring in positions 1–5 and in positions 11–15 along the block, and also the deviant presentations, when they occurred within these trial ranges, and compared the responses to these presentations with and without light. The average change in responses because of light in trials 11–15 was larger than the average change in trials 1–5 (Fig. 12*B*, Table 17, Pyramidal neurons section, main effect of "Chunk"). The responses of PV neurons, on the other hand, were affected similarly by the light in standard trials 11–15 compared with trials 1–5 (Fig. 12*C*,*D*, Table 17, PV neurons section).

We propose the following scenario to account for this observation. The first standard evokes a strong response in all neurons. In particular, the excitatory drive from the thalamocortical synapses on pyramidal neurons is so large that it is not affected strongly by inhibition. This strong response, however, causes a significant depression of the thalamocortical synapses as well as of both excitatory and inhibitory corticocortical synapses. In consequence, for the next few stimuli, the synapses of PV neurons on pyramidal neurons are depressed to the extent that PV suppression does not affect many of the pyramidal neurons. Eventually, the low levels of activation of PV neurons by standards allow these synapses to partially recover, and PV activity affects the pyramidal neurons.

Table 11. Effects of light on arch-expressing VIP neurons

			Range 0–40 ms[a]	
Term	Df1	Df2	*F*	*p*
ANOVA results				
(Intercept)	1	75	4.99	0.028
Condition	4	75	1.69	0.16

All factors as described above. Data are from seven neurons. Model: Difference ~ Condition + (1|cell:f).
[a]No significant modulation found for 40–150 or 0–150 ms.

Table 12. Effects of VIP suppression on the fast-spiking population

			Range 0–40 ms		Range 40–100 ms	
Term[a]	Df1	Df2	*F*	*p*	*F*	*p*
ANOVA results						
(Intercept)	1	105	0.951	0.33	2.82	0.096
Condition	4	105	3.00	0.022	2.03	0.096
Coefficient test results[b]						
$\Delta S = S_L - S_{NL}$	1	105	4.71	0.032		
$\Delta D = D_L - D_{NL}$	1	105	1.09	0.30		
$\Delta DB = DB_L - DB_{NL}$	1	105	6.94	0.0097		
$\Delta R = R_L - R_{NL}$	1	105	0.951	0.33		
$\Delta D - \Delta S$	1	105	6.77	0.011		
$\Delta D - \Delta DB$	1	105	5.17	0.025		

All factors as described above. S, Standard; D, deviant; DB, diverse broad; R, rare; L, light; NL, no light. These are two-sided tests performed to check whether the difference is significant for different conditions, and whether there are significant differences between differences of specific pairs of conditions. Data are from 11 neurons.
[a]The same model was selected for both time ranges: Difference ~ Condition + (1|cell:f).
[b]Intercept and condition terms were not significant according to the ANOVA, therefore no coefficient tests results are reported for the range 40–100 ms.

Table 13. Effects of VIP suppression on the pyramidal population

			Range 0–40 ms		Range 40–100 ms	
Term[a]	Df1	Df2	*F*	*p*	*F*	*p*
ANOVA results						
(Intercept)	1	81	0.180	0.67	0.0421	0.84
Condition	4	81	0.611	0.66	0.804	0.53

All factors as described above. Data are from nine neurons.
[a]The same model was selected for both time ranges: Difference ~ Condition + (1|cell:f).

Summary of the results

Figure 13 summarizes our findings, plotting the early and late responses of the four neuronal populations we studied

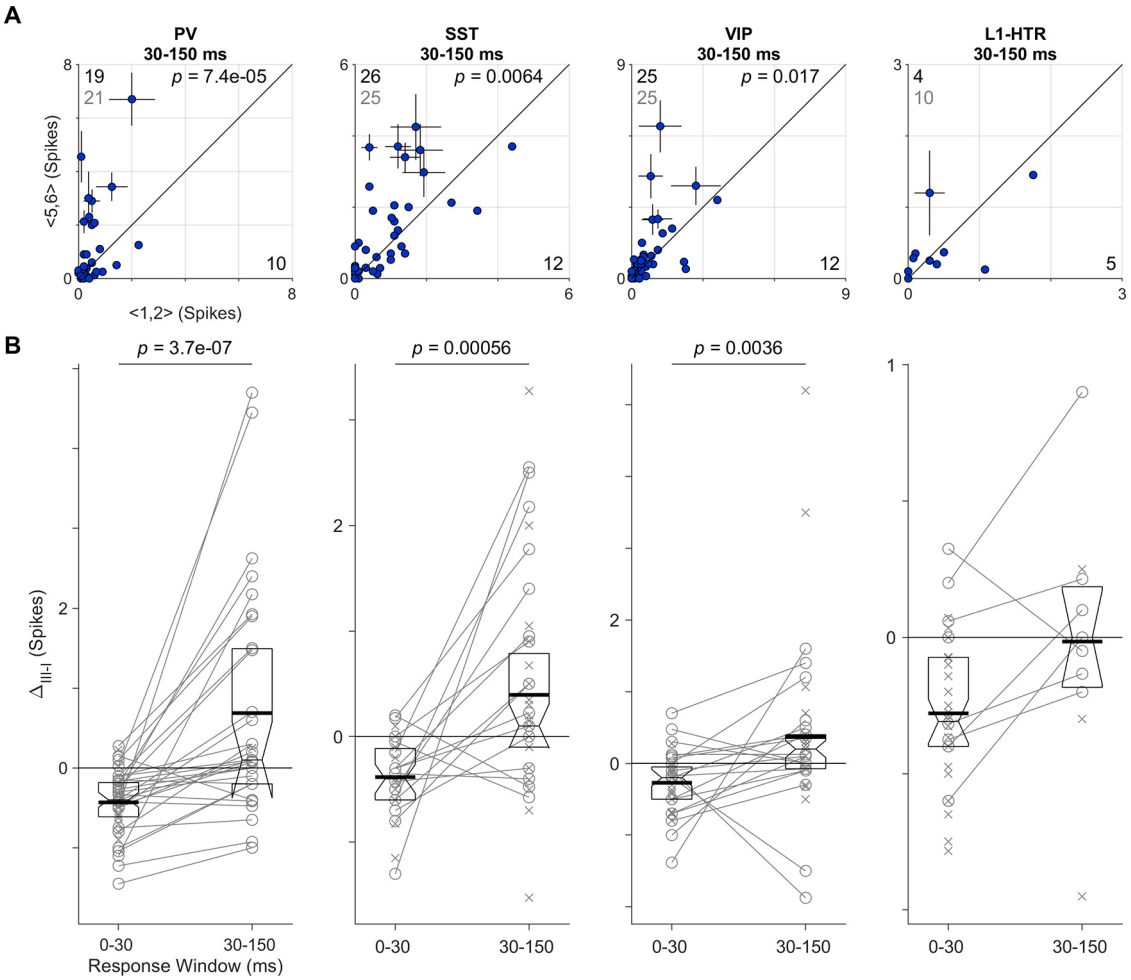

Figure 11. Inhibitory neurons show both adapting and facilitating responses to standard tones. ***A***, The average response to standard tones occurring in the fifth and sixth trials of each block (third pair) versus the average response to the first and second trials (first pair), in the four inhibitory populations (spikes counted between 30 and 150 ms after tone onset). Points below the diagonal represent adapting responses, while points above the diagonal represent facilitating responses. The numbers on each panel count the responses above and below diagonal (black), and of the neurons contributing these responses (gray). Error bars are SEMs. Populations where the response to the third pair differed significantly from the responses to the first pair are marked by showing the *p*-value for the corresponding coefficient test (Table 15). Standard responses were included in a panel only when the tone evoked significant responses in at least one of the three conditions: standard, deviant, or rare. Thus, each neuron contributes 0, 1, or 2 points to the scatter. ***B***, Δ_{III-I}, the difference between the responses to the third pair of trials (trials 5 and 6) and those to the first pair (trials 1 and 2), by response phase, in the four populations shown in ***A***. Gray lines connect cases where the average response to a tone was included in both the 0–30 ms and 30–150 ms time ranges; gray circles show the cases where the response was included in both ranges, and "x" marks the cases where the responses was significant only in one of the two ranges. Thus, most PV neurons were included in both response ranges, while in the populations of SST and VIP neurons many cases were included only in the late time range; L1-HTR neurons show predominantly early responses with no late component (as noted above, this group did not show a significant late response to any condition). Thick horizontal bars show the mean over the significant responses in each response phase; boxes mark the interquartile range with a notch at the median. Black lines above the plot mark the populations that had a significant difference between Δ_{III-I} of the third pair and Δ_{III-I} of the first pair, with the *p*-value of the corresponding coefficient test (Table 15).

(in color) as well as the effects of the suppression of two of these populations, PV and VIP interneurons, at four time points along an Oddball sequence. We made two important novel observations: the widespread occurrence of late responses in L2/3 inhibitory interneurons (PV, SSA, and VIP; see the large size of the late response bar for these populations starting with the standard preceding the first deviant); and the condition-specific effects of the suppression of these populations—suppressing PV responses affected the responses of pyramidal neurons to deviants more than to standards (Fig. 13, illustrated by the much higher effect of optogenetic suppression on the responses to the first deviant relative to the effects on the responses of the deviants), and suppressing VIP responses affected the responses of PV neurons to standards more than to deviants.

Table 14. Dynamics of standard responses in the 0–150 ms range

ANOVA results[a]	Term	Df1	DF2	*F*	*p*
All responses	Pair	2	555	4.47	0.035
	Population	3	555	3.89	0.0096
	Pair:Population	6	555	1.46	0.22
Including only responses to pairs (1, 2) and (5, 6)	Pair	1	370	1.42	0.23
	Population	3	370	8.93	1.0e-5
	Pair:Population	3	370	1.37	0.25
Including only responses to pairs (5, 6) and (94, 95)	Pair	1	370	24.4	2.6e-28
	Population	3	370	9.80	3.1e-6
	Pair:Population	3	370	2.27	0.080

Pair, Pair of trials along the block on which the response was averaged (Trials 1 and 2, 5 and 6, or 94 and 94); All other factors as described in previous tables; Response, difference between the responses to pairs I and III in the 0–150 ms range. Responses were collected from 26 PV, 30 SST, 30 VIP, and 22 L1-HTR neurons.

[a]Model used: Response ~ Pair*Population + (1|cell:f).

Table 15. Dynamics of standard responses for the early and late response ranges

	Term	Df1	Df2	*F*	*p*
ANOVA results	Pair	1	556	10.6	0.0012
	Range	1	556	33.6	1.1e-8
	Population	3	556	10.6	8.9e-7
	Pair:Range	1	556	26.5	3.7e-7
	Pair:Population	3	556	0.298	0.83
	Range:Population	3	556	8.66	1.3e-5
	Pair:Range:Population	3	556	1.78	0.15
Coefficient tests results	Estimate ± SE (Spikes)	Df1	Df2	*F*	*p*
Δ_{III-I}(0-30 ms)					
PV	−0.43 ± 0.13	1	556	10.6	0.0012
SST	−0.38 ± 0.17	1	556	4.98	0.026
VIP	−0.27 ± 0.16	1	556	3.04	0.082
L1-HTR	−0.28 ± 0.15	1	556	3.39	0.066
Δ_{III-I}(0-30 ms)					
PV	0.69 ± 0.17	1	556	15.9	7.4e-5
SST	0.40 ± 0.14	1	556	7.50	0.0064
VIP	0.37 ± 0.15	1	556	5.75	0.017
L1-HTR	−0.02 ± 0.29	1	556	0.00283	0.96
Δ_{III-I}(30-150 ms) > Δ_{III-I}(0-30 ms)					
PV	1.12 ± 0.22	1	556	26.5	3.7e-7
SST	0.78 ± 0.22	1	556	12.0	5.6e-4
VIP	0.64 ± 0.22	1	556	8.55	0.0036
L1-HTR		Δ_{III-I} was not significant in either range			

Response, Number of spikes within the time range; Pair, pair of trials along the block on which the response was averaged (I or III); Range, time range for counting spikes, 0–30 or 30–150 ms after stimulus onset (other factors as in previous tables); Δ_{III-I}(Range), difference between the responses to pairs I and III in the specified range. Responses were collected from 27 PV, 31 SST, 34 VIP, and 24 L1-HTR neurons. Model used: Response ~ Pair * Range * Population + (1|cell:f).

Table 16. Dynamics of standard responses, including only responses that were significant in both time ranges

	Term	Df1	Df2	*F*	*p*
ANOVA results	Pair	1	276	4.47	0.035
	Range	1	276	21.5	5.5e-6
	Population	3	276	3.89	0.0096
	Pair:Range	1	276	16.1	7.7e-5
	Pair:Population	3	276	0.200	0.90
	Range:Population	3	276	6.12	4.8e-4
	Pair:Range:Population	3	276	1.46	0.22
Coefficient tests results	Estimate ± SE (Spikes)	Df1	Df2	*F*	*p*
Coefficient tests results[a]					
PV	1.12 ± 0.28	1	276	16.1	7.7e-5
SST	1.11 ± 0.38	1	276	8.55	0.0038
VIP	0.39 ± 0.35	1	276	1.24	0.27
L1-HTR	0.24 ± 0.54	1	276	0.202	0.65

All factors as above. Responses were collected from 20 PV, 10 SST, 14 VIP, and 7 L1-HTR neurons. Model used: Response ~ Pair * Range * Population + (1|cell:f).
[a]ΔIII-I(30–150 ms) > ΔIII-I(0–30 ms). Fitting only cell–frequency pairs with both significant early and late responses.

Discussion

We present here an extensive survey of the inhibitory interneurons in the supragranular layers during SSA.

Relationships to previous studies

The existence of SSA in the PV and SST populations of A1 was demonstrated by Chen et al. (2015) and by Natan et al. (2015). Some of our results reproduce those of Chen et al. (2015). We found a similar reduction in responses to the first deviant, relative to responses to the first standard, in PV and SST neurons (by a factor of ~0.7; compare Fig. 7); and a rapid adaptation to the standards, occurring mostly within the first few stimuli.

Our results differ substantially from those of Natan et al. (2015), who found that PV interneurons similarly suppress standard and deviant responses. When using their analysis methods, firing rate changes because of light in our data were ~5–10 times larger for deviants than for standards (Fig. 9*I*,*J*). While there are a number of differences between the findings of Natan et al. (2015) and those of the current study, we suggest that the diverging results are largely because of differences in the level of optogenetic activation. The high level of inhibitory suppression in the study by Natan et al. (2015) caused a substantial increase in spontaneous activity (+0.12 in normalized mean firing rate) preceding stimulus onset in the non-PV (presumed pyramidal) neurons, which was almost as large as the increase in firing rate during stimulus presentation (+0.15; Natan et al., 2015, their Fig. 4*A*). In consequence, the responses to deviant tones in their light-on trials could be reduced because of spike-frequency adaptation or cortico-cortical synaptic depression, caused by the increased spontaneous activity. In contrast, in our experiments spontaneous activity showed only a minor perturbation on light onset (+0.02 to 0.06), while the responses to, for example, deviants at the high light intensities increased by more than 10-fold that amount (Fig. 9*I*,*J*). The high-power optogenetic activation used by Natan et al. (2015) could also affect inhibition outside L2/3, causing an increase in interlaminar input. This increase could potentially be stronger than the optogenetic effect in the recorded layer (Moore et al., 2018), further complicating the interpretation of their results. Thus, we believe our results are more relevant to the normal physiological function of interneurons and better reflect the possibilities of controlling SSA by inhibition in natural conditions.

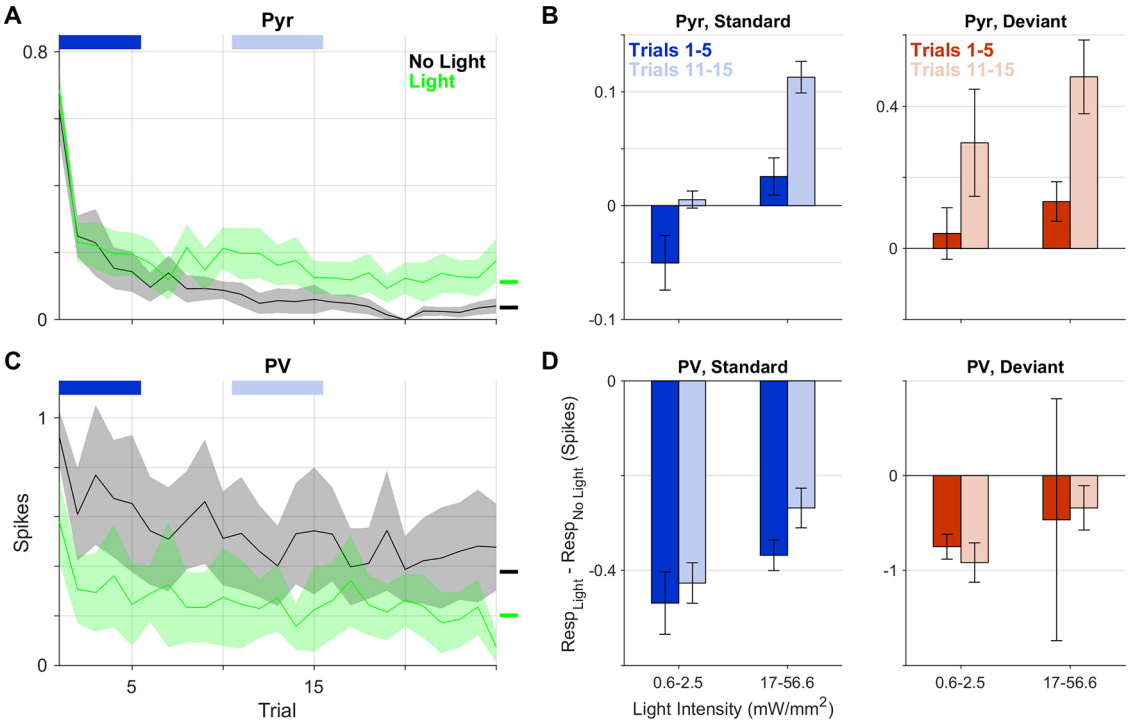

Figure 12. Disinhibition buildup at the beginning of the Oddball blocks. ***A***, The average response of pyramidal neurons during the 0–40 ms phase to standard tones appearing in the initial part of the block, without (black) and with (green) light stimulation of the highest intensity range, in animals expressing Arch in PV neurons (compare Fig. 8). Bands mark SEMs. The horizontal bars to the right of the plot mark the mean responses over the whole block in the no-light (black) and light (green) conditions. Blue and light blue bars above the curves show averaging ranges for the bar plots in ***B***. ***B***, Left, The difference between responses of pyramidal neurons with and without light, averaged over all standard tone presentations that occurred in trials 1–5 along the block (darker blue) and in trials 11–15 (light blue), in the lowest and the highest ranges of light intensity from Figure 8. Right, The difference between responses with and without light, averaged over responses to deviant presentations that occurred in trials 1–5 (red) and 11–15 (pink), in the same light intensity ranges. Error bars show SEMs over the population. Disinhibition was consistently stronger for the later period. ***C***, Same as ***A***, but for PV neurons expressing the Arch. ***D***, Same as ***B***, but for PV neurons. Suppression of PV responses was similar in the two ranges of trials (Table 17). Note the different *y*-scale in ***B*** and ***D***.

Table 17. Effects of light intensity along block

Term	Df1	Df2	*F*	*p*
Pyramidal neurons (range: 0–40 ms)				
Standard condition (ANOVA results)				
Chunk	1	307	13.7	2.5e-4
Light	1	307	25.6	7.2e-7
Deviant condition (ANOVA results)				
Chunk	1	132	7.14	0.0085
Light	1	132	2.15	0.14
PV neurons (range: 0–40 ms)				
Standard condition (ANOVA results)				
Chunk	1	166	2.44	0.12
Light	1	166	2.79	0.097
Deviant Condition (ANOVA Results)				
Chunk	1	58	0.017	0.90
Light	1	58	3.95	0.052

Difference, Difference in responses (in spikes) between light and no-light conditions; Chunk, group of trials within the block on which the difference is calculated (trials 1–5 or 11–15). Light, light intensity. Data are from 25 pyramidal and 13 PV neurons. Model used: Difference ~ Chunk + Light + (1|cell).

Our study was conducted under sevoflurane anesthesia, similar to many studies of SSA in anesthetized animals using halothane (Ulanovsky et al., 2003; Taaseh et al., 2011; Hershenhoren et al., 2014) and isoflurane (Chen et al., 2015; Natan et al., 2015). Given the similarity between SSA in the awake and the anesthetized states (Parras et al., 2017; Polterovich et al., 2018), we expect similar effects in awake animals. We note that while SSA is somewhat weaker in awake rats than in halothane-anesthetized rats (Polterovich et al., 2018), it is somewhat stronger in awake mice than in urethane-anesthetized rats (Parras et al., 2017). Both the anesthesia type and the species may affect these comparisons.

SSA in inhibitory populations of A1

Our results reveal novel properties of cortical inhibition in SSA. First, we studied two additional inhibitory subpopulations: the L2/3 VIP neurons, and the L1 inhibitory neurons. The average response profiles of L2/3 interneuron populations (PV, SST, and VIP) were similar, showing early-onset SSA and substantial late activity, which outlasted stimulus onset by ~100 ms and was often stronger for standard tones (Fig. 4). This is the first report of a consistent preference of cortical response components to the standard condition, and we report the facilitation of these late responses during the initial trials of each block (Figs. 6, 11). Since late responses did not occur in the L2/3 pyramidal neurons, the late responses may originate in other cortical layers, in distant cortical sources, or in subcortical sources. Alternatively, these late responses may reflect intrinsic mechanisms in the interneurons themselves.

Remarkably, inhibitory neurons could account for over half the spikes evoked by pure tones in L2/3 (Fig. 5). There may be a condition-specific change in the ratio between excitatory and inhibitory spiking activities when the cortex adapts to repeating stimuli. This has implications for extracellular recordings from A1. Even after fast-spiking units are identified by their extracellular spike shape, other types of interneurons may account for approximately one-quarter of the other spikes evoked by deviants and approximately one-half of those evoked by standards.

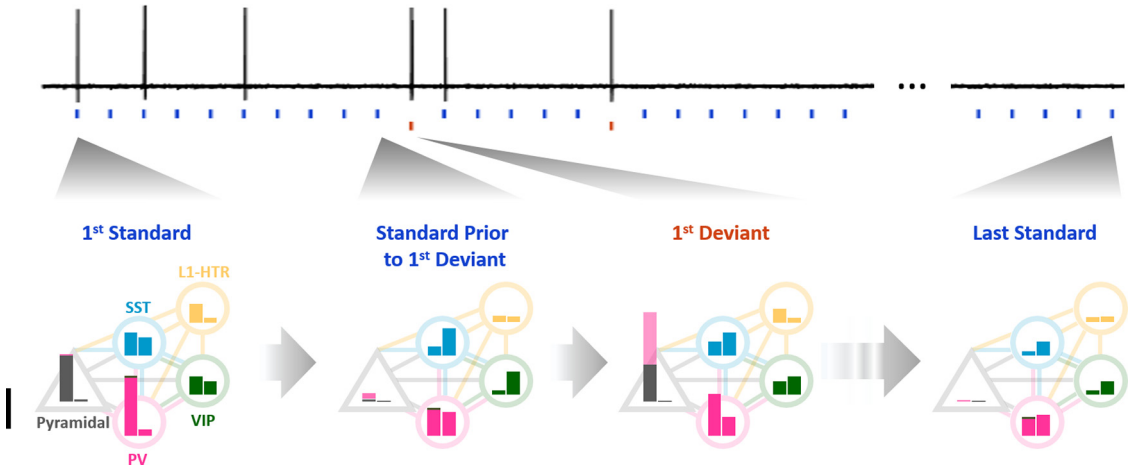

Figure 13. Stimulus-specific adaptation in the excitatory–inhibitory network (summary of results). Top, Responses of a pyramidal neuron to an Oddball protocol (the same trace as the no-light condition in Fig. 9*A*). Bottom, The responses in each of the populations we recorded from to four types of events, or trials, during the Oddball protocol (four of the five types of trials presented in Fig. 7). For each population, two bars represent the average number of spikes during the early response phase (0–30 ms for the inhibitory population, 0–40 ms for the pyramidal; left) and the late response phase (30–150 and 40–150 ms; right). The black bar on the left marks the unit of one spike for scale. The pink areas above the bars of the pyramidal neurons show the increase in the responses found under optogenetic suppression of the PV population (highest light intensity range): deviant responses were increased very strongly, while standard responses, and especially that to the first standard, showed only a small increase in the average number of spikes. Green areas on the top of the PV response bars show the effect of optogenetic suppression of the VIP population: reduction in standard but not in deviant responses.

Network reorganization by repeated stimulus presentations

Beyond the adaptation of early-phase standard responses, the neural activity during the first ~10 stimulus presentations showed two other important features.

The late responses to standards in L2/3 interneurons showed facilitation. For SST neurons, such facilitation was expected because their excitatory inputs show synaptic facilitation (Levy and Reyes, 2012). It was indirectly inferred from optogenetic manipulations (Natan et al., 2015; Phillips et al., 2017). Unexpectedly, facilitation of late sensory responses was also observed in PV and VIP neurons (Levy and Reyes, 2012; Karnani et al., 2016).

Furthermore, on average, responses of pyramidal neurons were barely affected by the suppression of PV responses during the first ~10 standard presentations. This is particularly surprising, since the PV neurons were suppressed from the first stimulus in the sequence, precisely when the PV-to-pyramidal synapse was presumably most effective [S1 (Heiss et al., 2008); A1 (Levy and Reyes, 2012)]. The apparent small effects of PV inhibition on the early standard trials may result from gradual partial recovery of PV-to-pyramidal synapses from their strong activation by the first standard and/or the temporary suppression of the excitatory network because of the depletion of its recurrent synapses on the first trial (Yarden and Nelken, 2017).

These observations suggest a significant reorganization of the cortical network during the first ~10 standard presentations, possibly because of the accumulation of synaptic depression and facilitation in both thalamocortical and corticocortical connections.

How does inhibition shape SSA?

Suppression of PV neurons caused a substantial increase in deviant responses (doubling their size), with 5–10 times smaller effects on standard responses (Fig. 9*I*,*J*). This was the case despite the robust PV responses to standards, and the similar suppression of PV responses to both standards and deviants. We suggest that the effectiveness of PV inhibition during standard presentations is reduced by depression of the PV-to-pyramidal synapse (Levy and Reyes, 2012), but that fresh PV neurons, not activated by the standards, are activated by deviants (Maor et al., 2016).

Our results show that responses of pyramidal neurons to standards are shaped mostly by reduction of the excitatory drive they receive. This reduction may occur because of synaptic depression or spike rate adaptation of their input neurons, either of which suffices to generate cortical SSA (Yarden and Nelken, 2017; Amsalem et al., 2020). Thus, the responses in the standard and deviant conditions can be differentially modulated by inhibition. Indeed, certain modulators of cortical inhibition (e.g., long-range corticocortical connections terminating on PV neurons; Schneider et al., 2014) or the cholinergic activation of L1 neurons, which inhibit PV neurons (Letzkus et al., 2011, 2015; Abs et al., 2018) may control SSA strength by specifically modifying deviant responses through their control of PV interneurons.

Suppressing VIP responses caused a decrease of PV responses to the standard and diverse broad conditions, but not to the deviant condition. VIP neurons affect PV neurons by direct inhibition and by indirect disinhibition through the VIP > SST > PV pathway (Pi et al., 2013; Askew and Metherate, 2016). The indirect effect was dominant: reducing VIP activity presumably increased the activity of SST neurons, thereby reducing PV responses.

One-third of our pyramidal neurons had deviant responses equivalent to or larger than responses to the same tones in the DB condition, suggesting some level of true deviance sensitivity (Taaseh et al., 2011). Such responses cannot be explained by a pure feedforward model of SSA (Taaseh et al., 2011). We argue that PV inhibition cannot account for such strong true-deviant responses in pyramidal neurons, as its suppression caused an equivalent increase in responses to deviants and to the same tones in the DB condition (Fig. 8, Table 8, Deviant and diverse broad responses only section). SST neurons probably cannot account for deviant-preferring pyramidal responses either: relatively more SST neurons showed preference for deviants over DB compared with pyramidal neurons (Table 3).

VIP neurons may control true deviance sensitivity. Their preference for tones in the DB condition could bias SST neurons

to prefer tones in the deviant condition, relative to the DB condition, with downstream effects on PV and pyramidal neurons. Control of VIP responses associated with the regulation of brain and behavioral states (Fu et al., 2014; Jackson et al., 2016; Pakan et al., 2016) may control true deviance sensitivity in pyramidal neurons through either SST or PV neurons. The stronger responses to deviants than to DB tones in the awake state (Polterovich et al., 2018) may be a consequence.

We conclude that, while the major signal generating cortical SSA is presumably a reduction of inputs during standard-tone presentations, the relative sizes of responses to standards, deviants, and the same tones in the diverse-broad condition are powerfully modulated by inhibition. Control of inhibition is therefore a viable way of controlling the strength of cortical responses to rare and deviant sounds.

References

Abolafia JM, Vergara R, Arnold MM, Reig R, Sanchez-Vives MV (2011) Cortical auditory adaptation in the awake rat and the role of potassium currents. Cereb Cortex 21:977–990.

Abs E, Poorthuis RB, Apelblat D, Muhammad K, Pardi MB, Enke L, Kushinsky D, Pu DL, Eizinger MF, Conzelmann KK, Spiegel I, Letzkus JJ (2018) Learning-related plasticity in dendrite-targeting layer 1 interneurons. Neuron 100:684–699.e6.

Amsalem O, King J, Reimann M, Ramaswamy S, Muller E, Markram H, Nelken I, Segev I (2020) Dense computer replica of cortical microcircuits unravels cellular underpinnings of auditory surprise response. bioRxiv. doi:10.1101/2020.05.31.126466.

Anderson LA, Christianson GB, Linden JF (2009) Stimulus-specific adaptation occurs in the auditory thalamus. J Neurosci 29:7359–7363.

Antunes FM, Nelken I, Covey E, Malmierca MS (2010) Stimulus-specific adaptation in the auditory thalamus of the anesthetized rat. PLoS One 5: e14071.

Askew CE, Metherate R (2016) Synaptic interactions and inhibitory regulation in auditory cortex. Biol Psychol 116:4–9.

Atallah BV, Bruns W, Carandini M, Scanziani M (2012) Parvalbumin-expressing interneurons linearly transform cortical responses to visual stimuli. Neuron 73:159–170.

Bäuerle P, von der Behrens W, Kössl M, Gaese BH (2011) Stimulus-specific adaptation in the gerbil primary auditory thalamus is the result of a fast frequency-specific habituation and is regulated by the corticofugal system. J Neurosci 31:9708–9722.

Chen IW, Helmchen F, Lütcke H (2015) Specific early and late oddball-evoked responses in excitatory and inhibitory neurons of mouse auditory cortex. J Neurosci 35:12560–12573.

Cohen L, Mizrahi A (2015) Plasticity during motherhood: changes in excitatory and inhibitory layer 2/3 neurons in auditory cortex. J Neurosci 35:1806–1815.

Duque D, Pérez-González D, Ayala YA, Palmer AR, Malmierca MS (2012) Topographic distribution, frequency, and intensity dependence of stimulus-specific adaptation in the inferior colliculus of the rat. J Neurosci 32:17762–17774.

Ewald AJ, Werb Z, Egeblad M (2011) Dynamic, long-term in vivo imaging of tumor-stroma interactions in mouse models of breast cancer using spinning-disk confocal microscopy. Cold Spring Harb Protoc 2011:pdb top97.

Fishman YI, Steinschneider M (2012) Searching for the mismatch negativity in primary auditory cortex of the awake monkey: deviance detection or stimulus specific adaptation? J Neurosci 32:15747–15758.

Fu Y, Tucciarone JM, Espinosa JS, Sheng N, Darcy DP, Nicoll RA, Huang ZJ, Stryker MP (2014) A cortical circuit for gain control by behavioral state. Cell 156:1139–1152.

Gothner T, Gonçalves PJ, Sahani M, Linden JF, Hildebrandt KJ (2021) Sustained activation of PV+ interneurons in core auditory cortex enables robust divisive gain control for complex and naturalistic stimuli. Cereb Cortex 31:2364–2381.

Grimm S, Escera C (2012) Auditory deviance detection revisited: evidence for a hierarchical novelty system. Int J Psychophysiol 85:88–92.

Heiss JE, Katz Y, Ganmor E, Lampl I (2008) Shift in the balance between excitation and inhibition during sensory adaptation of S1 neurons. J Neurosci 28:13320–13330.

Hershenhoren I, Taaseh N, Antunes FM, Nelken I (2014) Intracellular correlates of stimulus-specific adaptation. J Neurosci 34:3303–3319.

Jackson J, Ayzenshtat I, Karnani MM, Yuste R (2016) VIP+ interneurons control neocortical activity across brain states. J Neurophysiol 115:3008–3017.

Ji XY, Zingg B, Mesik L, Xiao Z, Zhang LI, Tao HW (2016) Thalamocortical innervation pattern in mouse auditory and visual cortex: laminar and cell-type specificity. Cereb Cortex 26:2612–2625.

Karnani MM, Jackson J, Ayzenshtat I, Tucciarone J, Manoocheri K, Snider WG, Yuste R (2016) Cooperative subnetworks of molecularly similar interneurons in mouse neocortex. Neuron 90:86–100.

Katz Y, Heiss JE, Lampl I (2006) Cross-whisker adaptation of neurons in the rat barrel cortex. J Neurosci 26:13363–13372.

Kaur S, Lazar R, Metherate R (2004) Intracortical pathways determine breadth of subthreshold frequency receptive fields in primary auditory cortex. J Neurophysiol 91:2551–2567.

Kurt S, Crook JM, Ohl FW, Scheich H, Schulze H (2006) Differential effects of iontophoretic in vivo application of the GABA(A)-antagonists bicuculline and gabazine in sensory cortex. Hear Res 212:224–235.

Lee S, Hjerling-Leffler J, Zagha E, Fishell G, Rudy B (2010) The largest group of superficial neocortical GABAergic interneurons expresses ionotropic serotonin receptors. J Neurosci 30:16796–16808.

Letzkus JJ, Wolff SB, Meyer EM, Tovote P, Courtin J, Herry C, Lüthi A (2011) A disinhibitory microcircuit for associative fear learning in the auditory cortex. Nature 480:331–335.

Letzkus JJ, Wolff SB, Lüthi A (2015) Disinhibition, a circuit mechanism for associative learning and memory. Neuron 88:264–276.

Levy RB, Reyes AD (2012) Spatial profile of excitatory and inhibitory synaptic connectivity in mouse primary auditory cortex. J Neurosci 32:5609–5619.

Liang F, Li H, Chou XL, Zhou M, Zhang NK, Xiao Z, Zhang KK, Tao HW, Zhang LI (2019) Sparse representation in awake auditory cortex: cell-type dependence, synaptic mechanisms, developmental emergence, and modulation. Cereb Cortex 29:3796–3812.

Malmierca MS, Cristaudo S, Pérez-González D, Covey E (2009) Stimulus-specific adaptation in the inferior colliculus of the anesthetized rat. J Neurosci 29:5483–5493.

Maor I, Shalev A, Mizrahi A (2016) Distinct spatiotemporal response properties of excitatory versus inhibitory neurons in the mouse auditory cortex. Cereb Cortex 26:4242–4252.

Maor I, Shwartz-Ziv R, Feigin L, Elyada Y, Sompolinsky H, Mizrahi A (2019) Neural correlates of learning pure tones or natural sounds in the auditory cortex. Front Neural Circuits 13:82.

Margrie TW, Meyer AH, Caputi A, Monyer H, Hasan MT, Schaefer AT, Denk W, Brecht M (2003) Targeted whole-cell recordings in the mammalian brain in vivo. Neuron 39:911–918.

Martenson M, Houts J, Heinricher M, Ogden B (2005) A simple device for humidification of inspired gases during volatile anesthesia in rats. Contemp Top Lab Anim Sci 44:46–48.

May PJ, Westö J, Tiitinen H (2015) Computational modelling suggests that temporal integration results from synaptic adaptation in auditory cortex. Eur J Neurosci 41:615–630.

Mill R, Coath M, Wennekers T, Denham SL (2011) A neurocomputational model of stimulus-specific adaptation to oddball and Markov sequences. PLoS Comput Biol 7:e1002117.

Moore AK, Weible AP, Balmer TS, Trussell LO, Wehr M (2018) Rapid rebalancing of excitation and inhibition by cortical circuitry. Neuron 97:1341–1355.e6.

Movshon JA, Lennie P (1979) Pattern-selective adaptation in visual cortical neurones. Nature 278:850–852.

Müller JR, Metha AB, Krauskopf J, Lennie P (1999) Rapid adaptation in visual cortex to the structure of images. Science 285:1405–1408.

Musall S, Haiss F, Weber B, von der Behrens W (2015) Deviant processing in the primary somatosensory cortex. Cereb Cortex 27:863–876.

Natan RG, Briguglio JJ, Mwilambwe-Tshilobo L, Jones SI, Aizenberg M, Goldberg EM, Geffen MN (2015) Complementary control of sensory adaptation by two types of cortical interneurons. eLife 4:e09868.

Natan RG, Rao W, Geffen MN (2017) Cortical interneurons differentially shape frequency tuning following adaptation. Cell Rep 21:878–890.

Netser S, Zahar Y, Gutfreund Y (2011) Stimulus-specific adaptation: can it be a neural correlate of behavioral habituation? J Neurosci 31:17811–17820.

Nieto-Diego J, Malmierca MS (2016) Topographic distribution of stimulus-specific adaptation across auditory cortical fields in the anesthetized rat. PLoS Biol 14:e1002397.

Nishikawa J, Ohtaka Y, Tachibana Y, Yanagawa Y, Osanai H, Haga T, Tateno T (2018) Flavoprotein fluorescence imaging-based electrode implantation for subfield-targeted chronic recording in the mouse auditory cortex. J Neurosci Methods 293:77–85.

Pakan JM, Lowe SC, Dylda E, Keemink SW, Currie SP, Coutts CA, Rochefort NL (2016) Behavioral-state modulation of inhibition is context-dependent and cell type specific in mouse visual cortex. eLife 5:e14985.

Parras GG, Nieto-Diego J, Carbajal GV, Valdés-Baizabal C, Escera C, Malmierca MS (2017) Neurons along the auditory pathway exhibit a hierarchical organization of prediction error. Nat Commun 8:2148.

Paxinos G, Franklin KBG (2003) The mouse brain in stereotaxic coordinates, Ed 2. Amsterdam: Elsevier Academic.

Phillips EAK, Hasenstaub AR (2016) Asymmetric effects of activating and inactivating cortical interneurons. eLife 5:e18383.

Phillips EAK, Schreiner CE, Hasenstaub AR (2017) Cortical interneurons differentially regulate the effects of acoustic context. Cell Rep 20:771–778.

Pi HJ, Hangya B, Kvitsiani D, Sanders JI, Huang ZJ, Kepecs A (2013) Cortical interneurons that specialize in disinhibitory control. Nature 503:521–524.

Polterovich A, Jankowski MM, Nelken I (2018) Deviance sensitivity in the auditory cortex of freely moving rats. PLoS One 13:e0197678.

Puccini GD, Sanchez-Vives MV, Compte A (2007) Integrated mechanisms of anticipation and rate-of-change computations in cortical circuits. PLoS Comput Biol 3:e82.

Rubin J, Ulanovsky N, Nelken I, Tishby N (2016) The Representation of Prediction Error in Auditory Cortex. PLoS Comput Biol 12:e1005058.

Schneider DM, Nelson A, Mooney R (2014) A synaptic and circuit basis for corollary discharge in the auditory cortex. Nature 513:189–194.

Shen L, Zhao L, Hong B (2015) Frequency-specific adaptation and its underlying circuit model in the auditory midbrain. Front Neural Circuits 9:55.

Taaseh N, Yaron A, Nelken I (2011) Stimulus-specific adaptation and deviance detection in the rat auditory cortex. PLoS One 6:e23369.

Tan AY, Zhang LI, Merzenich MM, Schreiner CE (2004) Tone-evoked excitatory and inhibitory synaptic conductances of primary auditory cortex neurons. J Neurophysiol 92:630–643.

Tan AY, Atencio CA, Polley DB, Merzenich MM, Schreiner CE (2007) Unbalanced synaptic inhibition can create intensity-tuned auditory cortex neurons. Neuroscience 146:449–462.

Tasaka GI, Guenthner CJ, Shalev A, Gilday O, Luo L, Mizrahi A (2018) Genetic tagging of active neurons in auditory cortex reveals maternal plasticity of coding ultrasonic vocalizations. Nat Commun 9:871.

Thomas JM, Morse C, Kishline L, O'Brien-Lambert A, Simonton A, Miller KE, Covey E (2012) Stimulus-specific adaptation in specialized neurons in the inferior colliculus of the big brown bat, Eptesicus fuscus. Hear Res 291:34–40.

Tremblay R, Lee S, Rudy B (2016) GABAergic interneurons in the neocortex: from cellular properties to circuits. Neuron 91:260–292.

Ulanovsky N, Las L, Nelken I (2003) Processing of low-probability sounds by cortical neurons. Nat Neurosci 6:391–398.

von der Behrens W, Bäuerle P, Kössl M, Gaese BH (2009) Correlating stimulus-specific adaptation of cortical neurons and local field potentials in the awake rat. J Neurosci 29:13837–13849.

Wang J, Caspary D, Salvi RJ (2000) GABA-A antagonist causes dramatic expansion of tuning in primary auditory cortex. Neuroreport 11:1137–1140.

Wang J, McFadden SL, Caspary D, Salvi R (2002) Gamma-aminobutyric acid circuits shape response properties of auditory cortex neurons. Brain Res 944:219–231.

Wehr M, Zador AM (2003) Balanced inhibition underlies tuning and sharpens spike timing in auditory cortex. Nature 426:442–446.

Wu GK, Li P, Tao HW, Zhang LI (2006) Nonmonotonic synaptic excitation and imbalanced inhibition underlying cortical intensity tuning. Neuron 52:705–715.

Wu GK, Arbuckle R, Liu BH, Tao HW, Zhang LI (2008) Lateral sharpening of cortical frequency tuning by approximately balanced inhibition. Neuron 58:132–143.

Xu X, Roby KD, Callaway EM (2010) Immunochemical characterization of inhibitory mouse cortical neurons: three chemically distinct classes of inhibitory cells. J Comp Neurol 518:389–404.

Yarden TS, Nelken I (2017) Stimulus-specific adaptation in a recurrent network model of primary auditory cortex. PLoS Comput Biol 13:e1005437.

Zeisel A, Muñoz-Manchado AB, Codeluppi S, Lönnerberg P, La Manno G, Juréus A, Marques S, Munguba H, He L, Betsholtz C, Rolny C, Castelo-Branco G, Hjerling-Leffler J, Linnarsson S (2015) Brain structure. Cell types in the mouse cortex and hippocampus revealed by single-cell RNA-seq. Science 347:1138–1142.